Supplementary Information

Continuous Direct Air Capture and Conversion Tandem System Applicable to a Wide Range of CO_2 Concentrations

Shinta Miyazaki[a], Akihiko Anzai[a,*], Masaki Yoshihara[a], Hsu Sheng Feng[a], Shinya Mine[b], Takashi Toyao[a], Ken-ichi Shimizu[a,*]

[a] Institute for Catalysis, Hokkaido University, N-21, W-10, Sapporo 001-0021, Japan

[b] Research Institute for Chemical Process Technology, National Institute of Advanced Industrial Science and Technology (AIST), 4-2-1, Nigatake, Miyagino-ku, Sendai 983-8551, Japan

*Corresponding author
Akihiko Anzai, E-mail: anzai.akihiko@cat.hokudai.ac.jp
Ken-ichi Shimizu, Email: kshimizu@cat.hokudai.ac.jp

Supplementary Figs and Supplementary Texts

Introduction

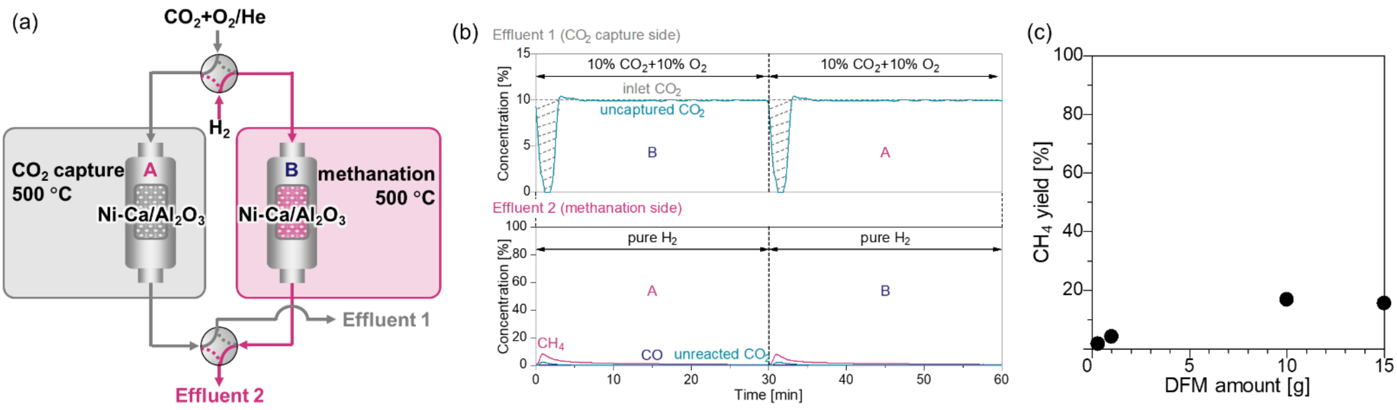

Supplementary Fig. 1 (**a**) Schematic diagram of the continuous CO_2 capture and methanation system; captured gas (100 mL/min, 10%CO_2+10%O_2/He for 30 min) and hydrogenation gas (100 mL/min, pure H_2 for 30 min) were alternately fed into each reactor containing 10 g of Ni-Ca/Al_2O_3 (**b**) Typical time course of the CH_4, CO_2, and CO concentration in effluent 1 and 2, respectively. (**c**) Variation in CH_4 yield with DFM amount in continuous CO_2 capture and methanation.

Supplementary Text 1

Previously, various DFMs for selective CH_4 production were reported. Especially, Ni-Ca based DFMs were well-known as high performance one (Supplementary Table 1 and 2). Recently, our group developed Ni-Ca/Al_2O_3 DFM, which optimized Ni and Ca loading. Detail characterization revealed that 500 ºC is the best condition for CO_2 capture and methanation. For continuous CH_4 production from high concentration of CO_2, we carried out CO_2 capture and methanation using the continuous CCR system (Supplementary Fig. 1a). First, the CO_2/O_2 mixture was fed into one reactor for 30 min for CO_2 capture. On the other hand, pure H_2 was fed into the other reactor (containing a CO_2-captured Ni-Ca/Al_2O_3). Supplementary Fig. 1b shows the typical time course of the CH_4, and CO_2 concentrations analyzed by online gas-cell IR in effluent 1 and 2, respectively. Supplementary Fig. 1c shows the result of the optimization of Ni-Ca/Al_2O_3 amount. These results indicate that increasing the amount of DFM has limited effects on improving CH_4 yield (<20%).

Results and Discussion

Screening and optimization of sorbents and catalysts

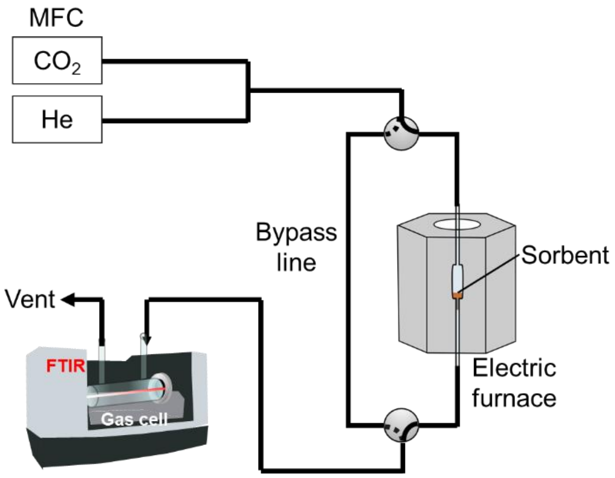

Supplementary Fig. 2 Illustration of the experimental setup for CO_2 adsorption measurement.

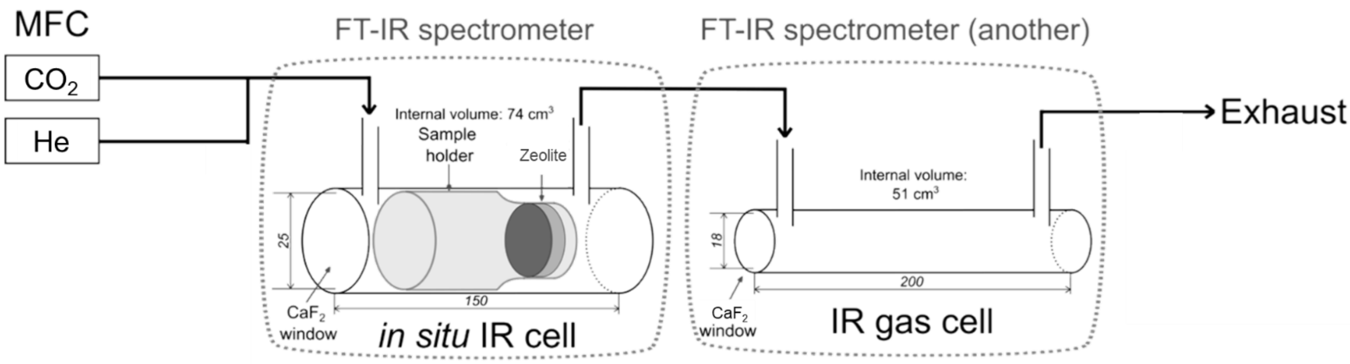

Supplementary Fig. 3 Schematic view of the setup used for *operando* IR measurement, including *in situ* IR cell and IR gas cell. The inner diameter and length of the cell are provided with a unit of mm.

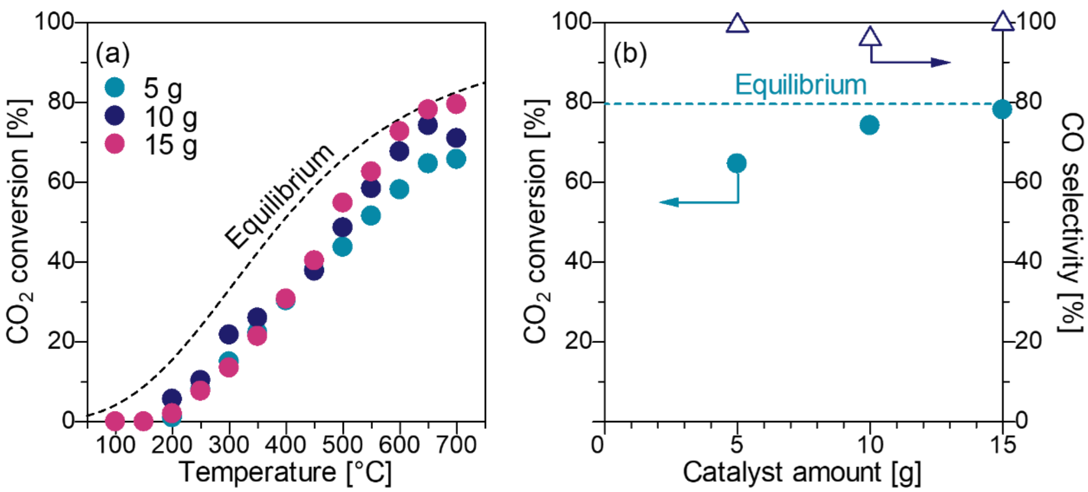

Supplementary Fig. 4 (a) Validation in CO_2 conversion with respect to temperature for different amounts of $Cu/ZnO/Al_2O_3$. (b) Variation in CO_2 conversion and CO selectivity with catalyst amount in steady-state RWGS reaction over $Cu/ZnO/Al_2O_3$.

Continuous production of O_2-free CO_2 from CO_2/O_2 mixture

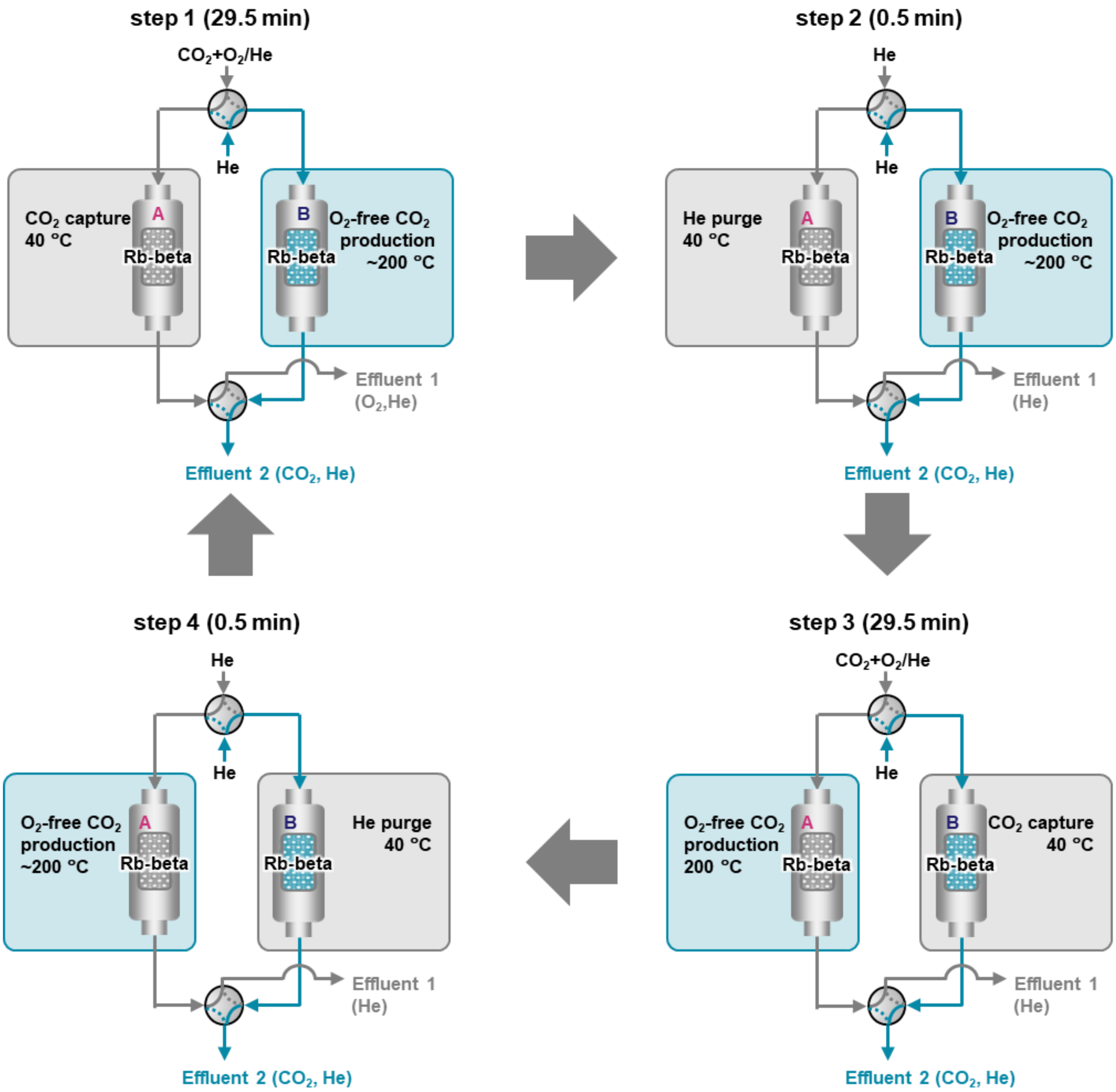

Supplementary Fig. 5 Schematic diagram and procedure of the continuous CO_2 capture and O_2-free CO_2 production.

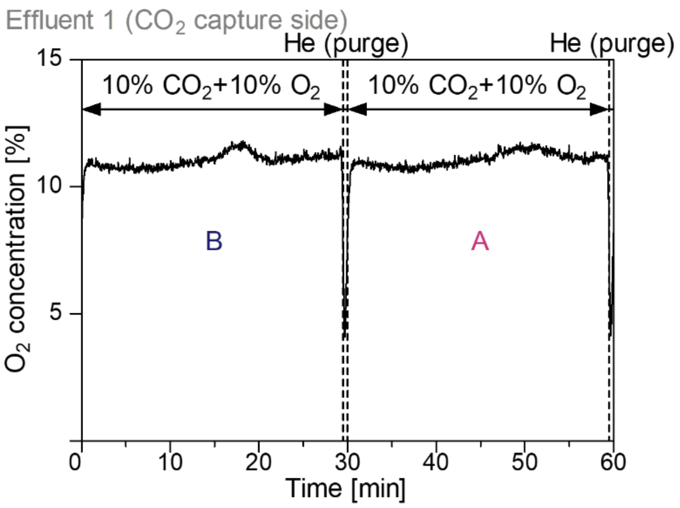

Supplementary Fig. 6 Typical time course of the O_2 concentration in effluent 1 during continuous CO_2 capture and O_2-free CO_2 production.

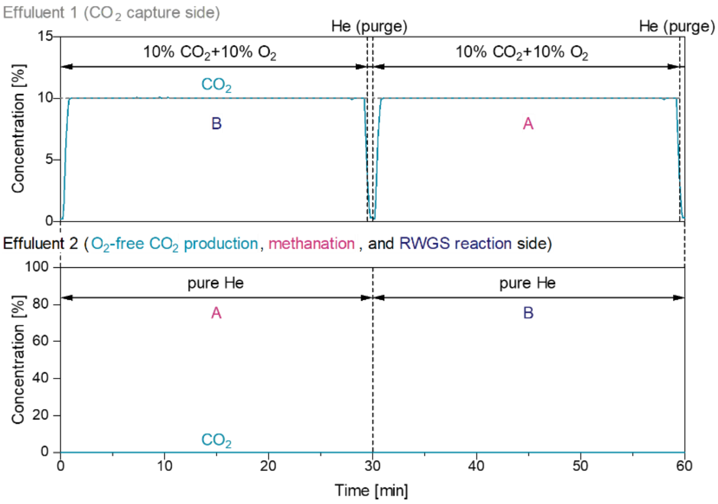

Supplementary Fig. 7 Effluent concentration profiles of CO_2 for blank during continuous CO_2 capture and O_2-free CO_2 production, methanation and. RWGS reaction side production; captured gas (100 mL/min, 10%CO_2+10%O_2/He for 29.5 min and then pure He for 0.5 min) and other side gas (120 mL/min, pure He for 30 min).

Supplementary Text 2

In continuous CO_2 capture and O_2-free CO_2 production, the total flow rate was moderately changed due to O_2-free CO_2 production. The total flow rate in effluent 2 can be shown eq. 1. The produced O_2-free CO_2 flow rate can be calculated in eq. 2. Finally, eq. 3 to derive the total flow rate was calculated from eqs. 1 and 2. The derived total flow rate is close to the measured total flow rate by the soap-film flow meter (HORIBA, Ltd., Fluid Control System SF-1U combined VP-3U, Supplementary Fig. 7). From eqs. 2 and 6, the amount of produced O_2-free CO_2 every 0.5 min was derived and O_2-free CO_2 yield was also calculated (O_2-free CO_2 yield = 97%, Supplementary Fig. 7).

$$F_{all}^{out(2)} = F_{CO2}^{out(2)} + F_{He}^{out(2)} \quad (1)$$

$$F_{CO2}^{out(2)} = C_{CO2}^{out(2)} \times F_{all}^{out(2)} \quad (2)$$

$$F_{all}^{out(2)} = \frac{F_{He}^{out(2)}}{1-C_{CO2}^{out(2)}} \quad (3)$$

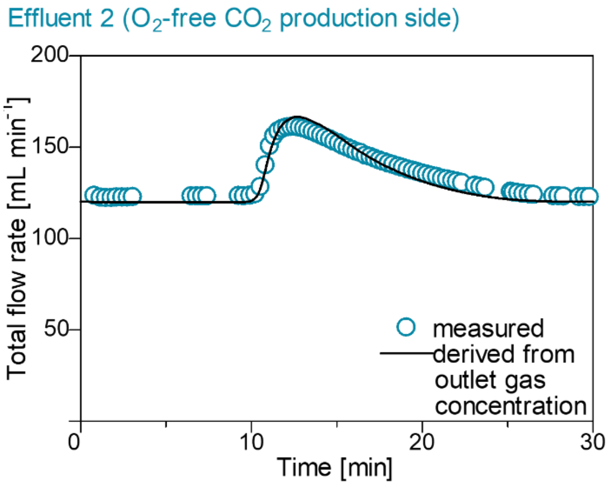

Supplementary Fig. 8 Comparison of changes about measured total flow rate and derived total flow rate from outlet gas concentration in effluent 2 during CO_2 capture and O_2-free CO_2 production. Conditions are the same as in Fig. 5. The methodology of total flow rate derivation from outlet gas concentration in effluent 2 is shown in Supplementary Text 1.

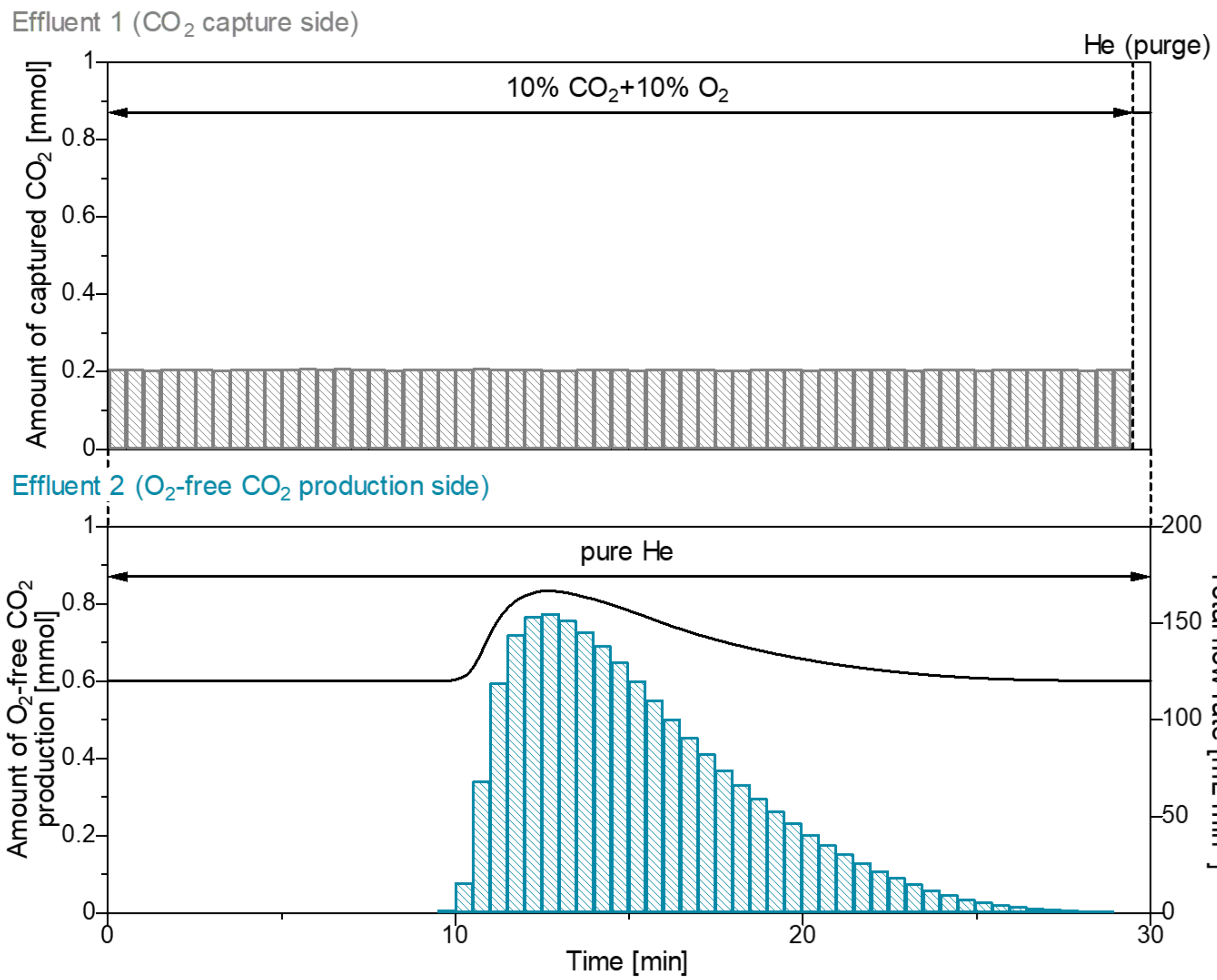

Supplementary Fig. 9 Time course of amount of captured CO_2 in effluent 1, O_2-free CO_2 production in effluent 2 every 0.5 min, and total flow rate of effluent 2 for continuous CO_2 capture and RWGS reaction. Conditions are the same as in Fig. 5.

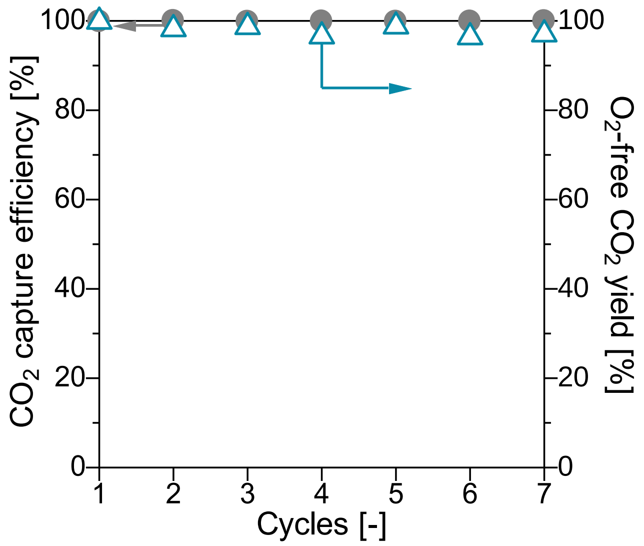

Supplementary Fig. 10 Transitions of the CO_2 capture efficiency and O_2-free CO_2 yield during cyclic test of continuous CO_2 capture and O_2-free CO_2 production. Conditions are the same as in Fig. 5.

Continuous CO_2 capture and methanation/RWGS reaction using the tandem system

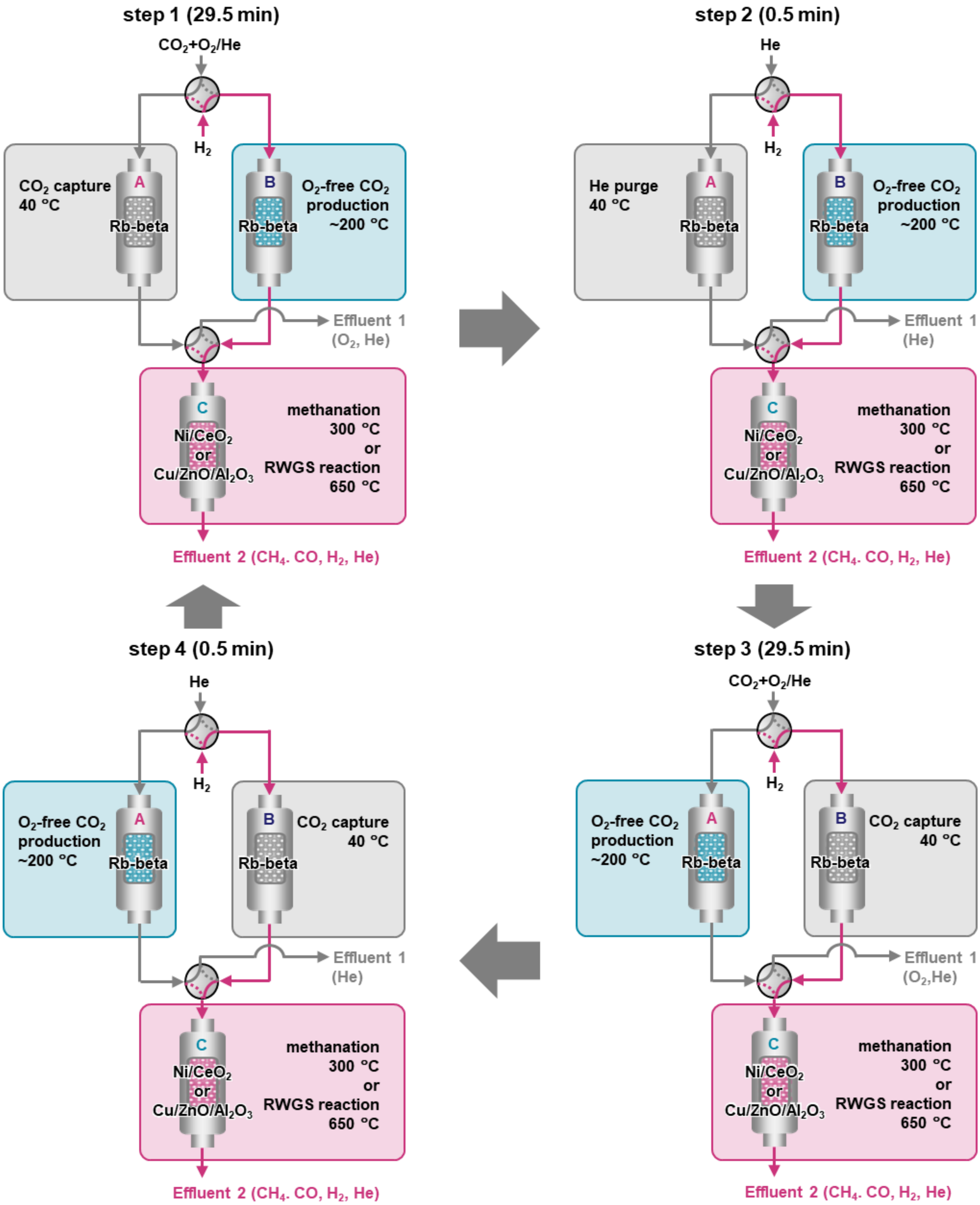

Supplementary Fig. 11 Schematic diagram and procedure of the continuous CO_2 capture and methanation as well as RWGS reaction.

Supplementary Text 3

In continuous high-concentration CO_2 capture and methanation, total flow rate was drastically changed due to large amount of CH_4 formation. The total flow rate in effluent 2 can be shown eq. 1, because of produced CO and unreacted CO_2 are hardly observed, and produced H_2O was captured by the cold trap. From the stochiometric equation of methanation (eq. 3 in Main Text), produced CH_4 and unreacted H_2 flow rates can be shown eqs. 2 and 3, respectively. amount of converted H_2 can be calculated by eq. 4 and eq. 4 can transformed to eq. 5 using eq. 2. Finally, eq. 6 to derive the total flow rate was calculated from eqs. 4 and 5. The derived total flow rate is close to the measured total flow rate by the soap-film flow meter (HORIBA, Ltd., Fluid Control System SF-1U combined VP-3U). From eqs. 2 and 6, the amount of produced CH_4 every 0.5 min was derived and CH_4 yield was also calculated (CH_4 yield = 92%, Supplementary Fig. 10).

$$F_{all}^{out(2)} = F_{CH4}^{out} + F_{H2}^{out} \tag{1}$$

$$F_{CH4}^{out} = C_{CH4}^{out} \times F_{all}^{out(2)} \tag{2}$$

$$F_{H2}^{out} = (1 - C_{CH4}^{out}) \times F_{all}^{out(2)} \tag{3}$$

$$F_{H2}^{in} - F_{H2}^{out} = 4 \times F_{CH4}^{out} \tag{4}$$

$$F_{H2}^{in} - F_{H2}^{out} = 4 \times C_{CH4}^{out} \times F_{all}^{out(2)} \tag{5}$$

$$F_{all}^{out} = \frac{F_{H2}^{in}}{1+3C_{CH4}^{out}} \tag{6}$$

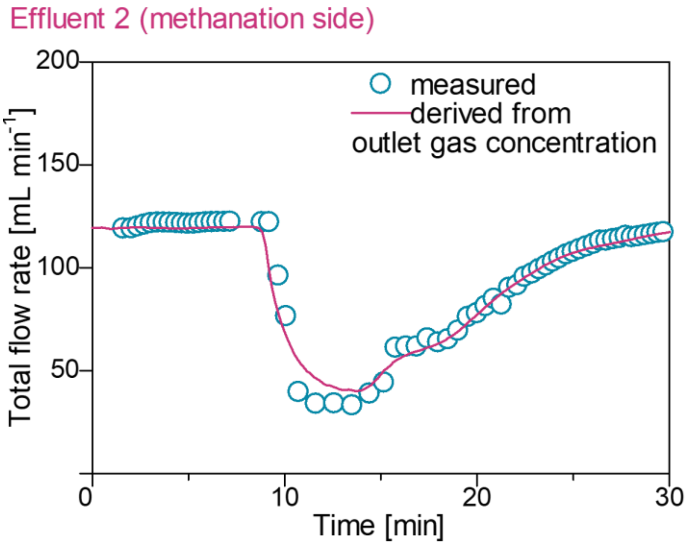

Supplementary Fig. 12 Comparison of changes about measured total flow rate and derived total flow rate from outlet gas concentration in effluent 2 during CO_2 capture and methanation. Conditions are the same as in Fig. 5. The methodology of total flow rate derivation from outlet gas concentration in effluent 2 is shown in Supplementary Text 3.

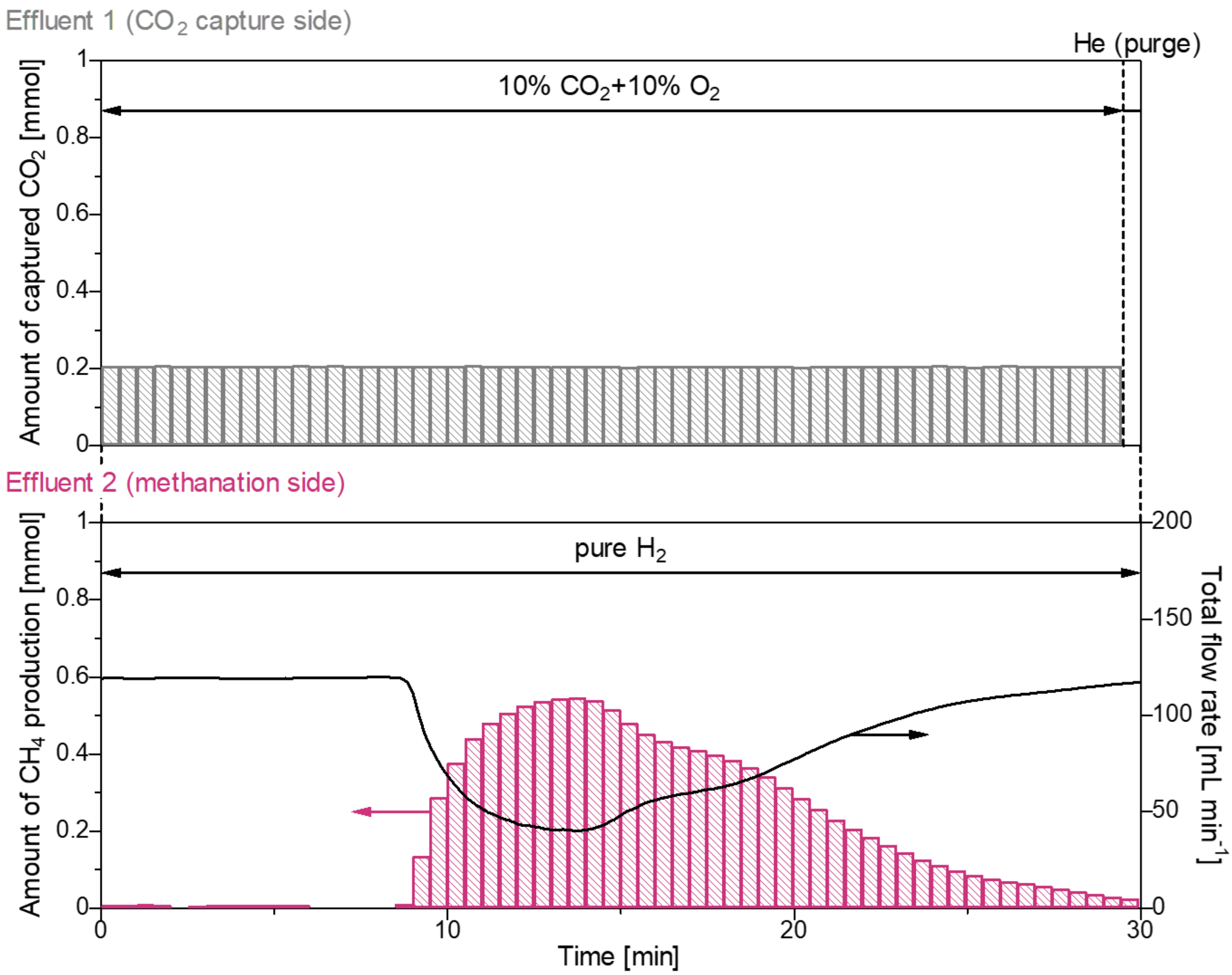

Supplementary Fig. 13 Time course of amount of captured CO_2 in effluent 1, CH_4 production in effluent 2 every 0.5 min, and total flow rate of effluent 2 for continuous CO_2 capture and methanation. Conditions are the same as in Fig. 5.

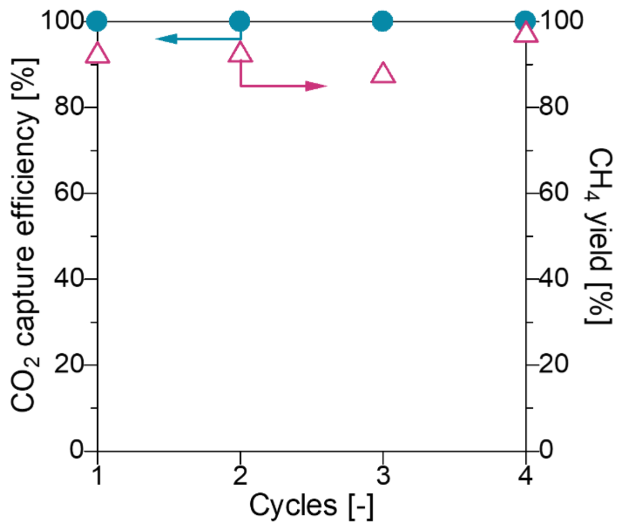

Supplementary Fig. 14 Transitions of the CO_2 capture efficiency and CH_4 yield during cyclic test of continuous CO_2 capture and RWGS reaction. Conditions are the same as in Fig. 5.

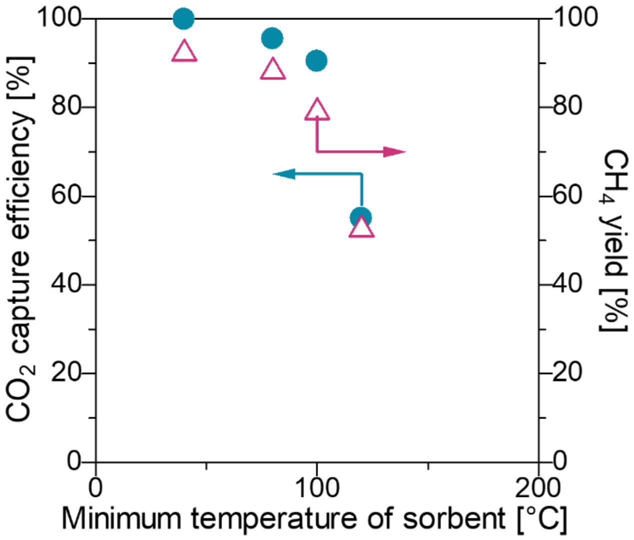

Supplementary Fig. 15 Variation in CO_2 capture efficiency and CH_4 yield with range of temperature changing (minimum range from 40 °C to 120 °C) in continuous CO_2 capture and CH_4 production.

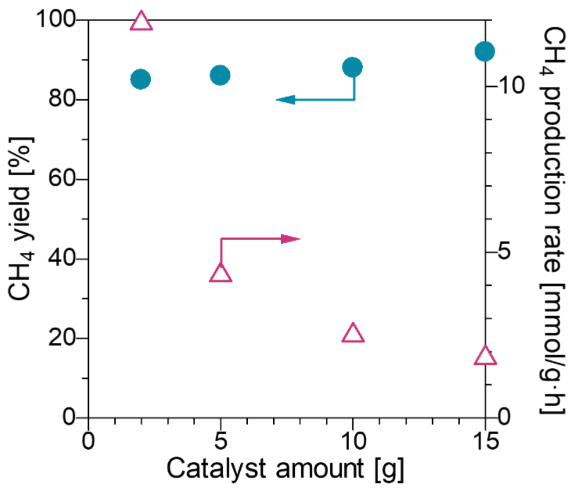

Supplementary Fig. 16 Variation in CH_4 yield and CH_4 production rate with catalyst amount in continuous CO_2 capture and CH_4 production.

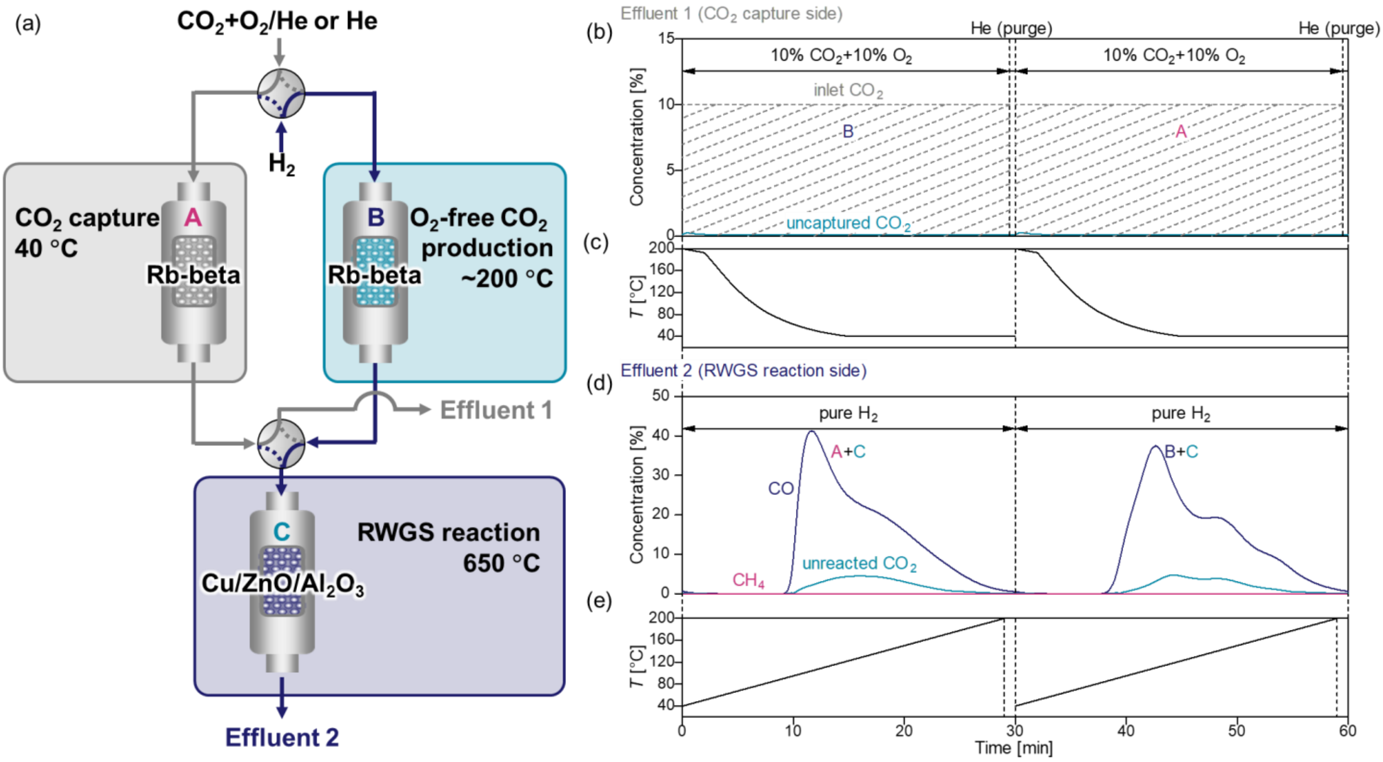

Supplementary Fig. 17 (a) Schematic diagram of the two-reactor TSA system for continuous CO_2 capture and RWGS reaction; captured gas (100 mL/min, 10%CO_2+10%O_2/He for 29.5 min and then pure He for 0.5 min) and hydrogenation gas (100 mL/min, pure H_2 for 30 min) were alternately fed into each reactor containing 14 g of Rb-beta (b and d) Typical time course of the CO_2 and O_2 concentration in effluent 1 and 2, respectively. (c and e) Typical time course of the temperature changing in reactor a and b, respectively.

__**Supplementary Text 4**__

In continuous high-concentration CO_2 capture and RWGS reaction, total flow rate was slightly changed due to CO formation and CO_2 desorption. Using the soap-film flow meter, total flow rate in effluent 2 was measured and the amount of produced CO every 0.5 min was derived, and CO yield was also calculated (CO yield = 85%, Supplementary Fig. 18).

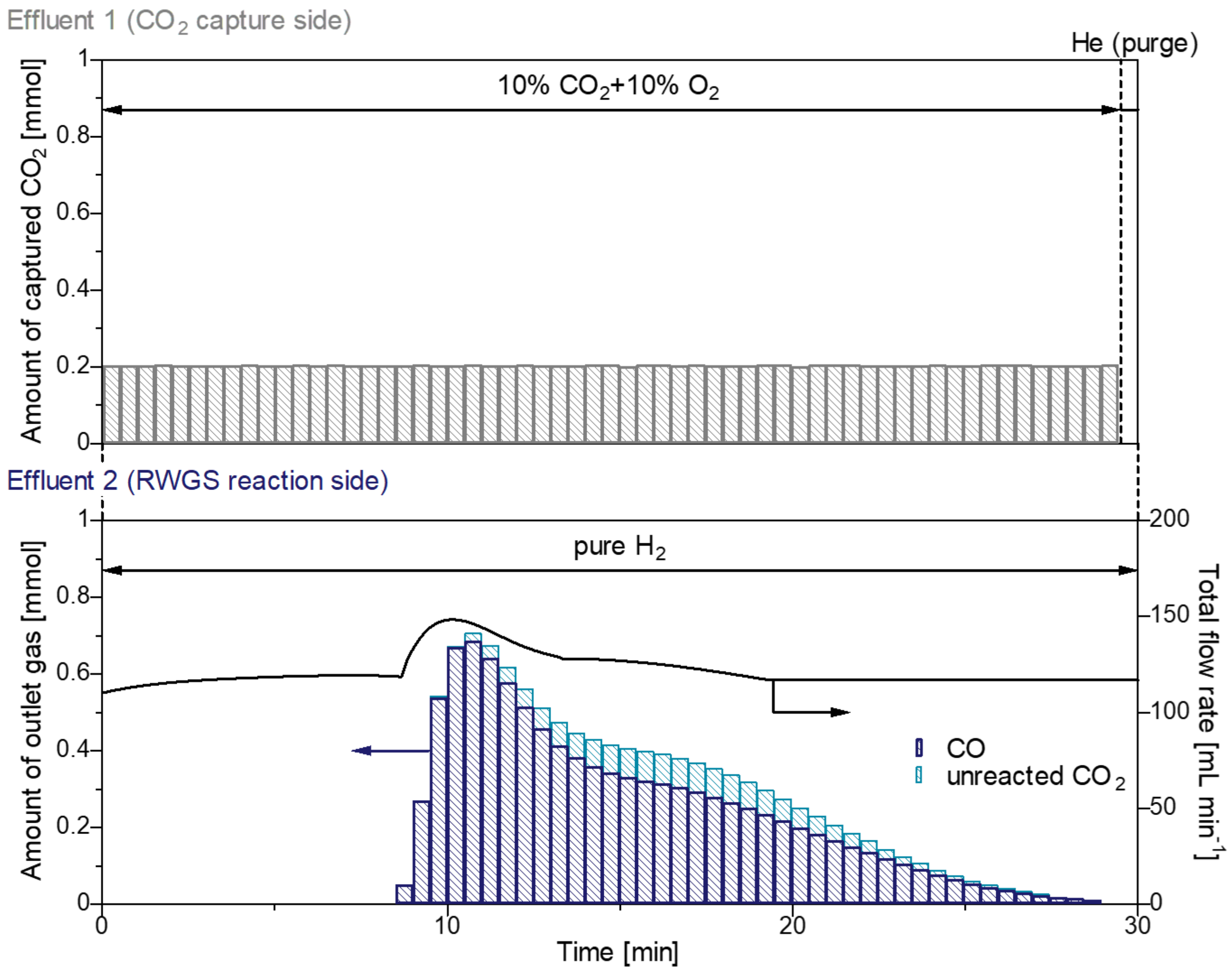

Supplementary Fig. 18 Time course of amount of captured CO_2 in effluent 1, CO production in effluent 2 every 0.5 min, and total flow rate of effluent 2 for continuous CO_2 capture and RWGS reaction. Conditions are the same as in Supplementary Fig. 17.

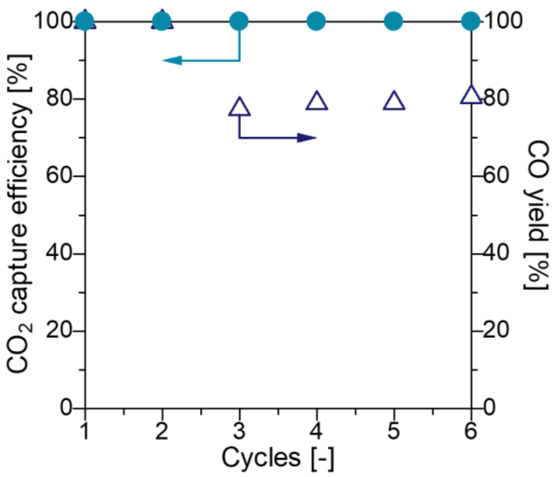

Supplementary Fig. 19 Transitions of the CO_2 capture efficiency and CO yield during the cyclic test of continuous CO_2 capture and RWGS reaction. Conditions are the same as in Supplementary Fig. 17.

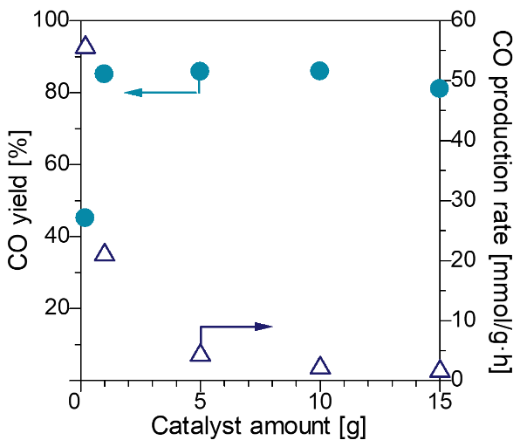

Supplementary Fig. 20 Variation in CO yield and STY_{CO} with catalyst amount in continuous CO_2 capture and RWGS Reaction.

Supplementary text 5

We demonstrated continuous CO_2 capture and methanation, with the H_2 flow time of H_2 reduced from 30 min to 20 min. Similar to Fig. 6, 10% CO_2 + 10% O_2 was fed into one reactor for 29.5 min for CO_2 capture with cooling, and then pure He (0.5 min) was fed to purge the remaining O_2 in the reactor and gas line (Supplementary Fig. 21a). At the same time, into the other reactor in parallel, pure H_2 was fed at 20 min after 10 min of no gas flow with heating. CO_2 capture efficiency and CH_4 yield were maintained during 4 cycles at 99% and 93%, respectively (Supplementary Fig. 21e). The effect of H_2 flow time was investigated and H_2 conversion and the average CH_4 concentration were increased from 38% to 58%, and from 9.8% to 15%, respectively.

Supplementary Text 6

H_2 conversion is also an important property in the CO_2 methanation process. We demonstrated continuous CO_2 capture and methanation, with the H_2 flow time of H_2 reduced from 30 min to 20 min. Similar to Fig. 6, 10% CO_2 + 10% O_2 was fed into one reactor for 29.5 min for CO_2 capture with cooling, and then pure He (0.5 min) was fed to purge the remaining O_2 in the reactor and gas line (Supplementary Fig. 21a). At the same time, into the other reactor in parallel, pure H_2 was fed at 20 min after 10 min of no gas flow with heating. CO_2 capture efficiency and CH_4 yield were maintained during 4 cycles at 99% and 93%, respectively (Supplementary Fig. 21e). The effect of H_2 flow time was investigated and H_2 conversion and the average CH_4 concentration were increased from 38% to 58%, and from 9.8% to 15%, respectively.

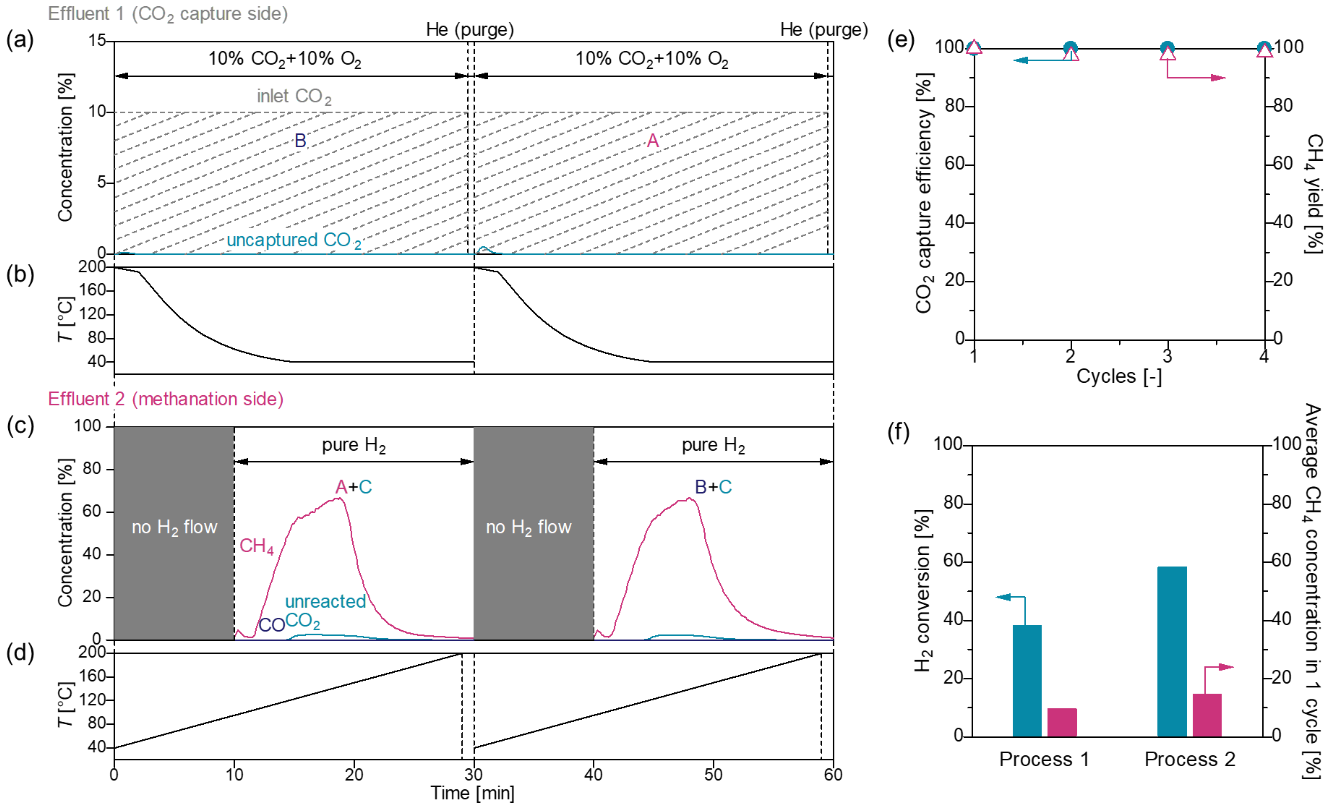

Supplementary Fig. 21 (a) Schematic diagram and procedure of the continuous CO_2 capture and methanation; captured gas (100 mL min^{-1}, 10% CO_2+10%O_2/He for 29.5 min and then pure He for 0.5 min) and hydrogenation gas (100 mL min^{-1}, pure H_2 for 20 min) were alternately fed into each reactor containing 14 g of Rb-beta. (b and d) Typical time course of the CH_4, CO_2, and CO concentration in effluent 1 and 2, respectively. (c and e) Typical time course of the temperature changing in reactor a and b, respectively. (f) Transitions of the CO_2 capture efficiency and CH_4 yield during cyclic test. (g) Comparison of H_2 conversion and average CH_4 concentration in 1 cycle between conditions of Fig. 6 (denoted as process 1) and conditions of Supplementary Fig. 21 (denoted as process 2).

Continuous direct air capture and methanation

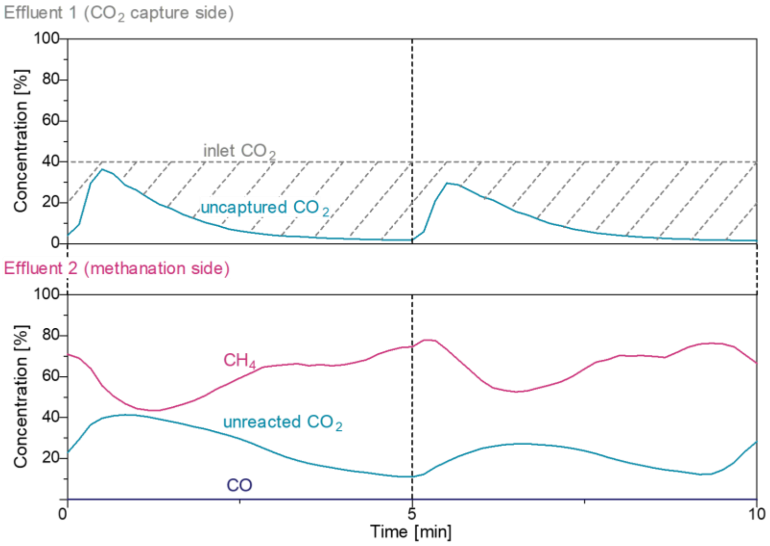

Supplementary Fig. 22 Typical time course of CH_4, CO, and unreacted CO_2 in effluent 2 for continuous high-concentration CO_2 capture and methanation. Conditions: 14 g of Rb-beta for each upper reactor, temperature swing from 80 °C to 100 °C (heating rate = 20 °C/min). 15 g of Ni/CeO_2 for the bottom reactor, 300 °C. 500 mL/min air for 5 min, switched to 10 mL min^{-1} H_2 for another 5 min.

Tables

Results and Discussion

Supplementary Table 1. Summary of the continuous CO_2 capture and methanation in this study and other reported CO_2 capture and methanation considering the effect of coexistent O_2.

DFMs or catalyst	CO_2 capture gas	Hydrogenation gas	CH_4 yield [%]	*T* [℃]	ref
Ni(5)/CeO_2	10%CO_2+10%O_2/He	100% H_2	92	300	*
Ru(1)-Ni(10)-Na_2O(6.1) /Al_2O_3	7.5%CO_2+4.5%O_2 +15%H_2O/N_2	15%H_2/N_2	5.67	320	[1]
Pt(1)-Ni(10)-Na_2O(6.1) /Al_2O_3	7.5%CO_2+4.5%O_2 +15%H_2O/N_2	15%H_2/N_2	3.73	320	[1]
Ru(1)-Na_2O(6.1) /Al_2O_3	7.5%CO_2+4.5%O_2 +15%H_2O/N_2	15%H_2/N_2	4.63	320	[1]
Ru(5)-Na_2O(6.1) /Al_2O_3	7.5%CO_2+4.5%O_2 +15%H_2O/N_2	15%H_2/N_2	4.35	320	[2]
Ni(10)-Na_2O(6.1) /Al_2O_3	7.5%CO_2+4.5%O_2 +15%H_2O/N_2	15%H_2/N_2	4.12	320	[2]
Ru(0.95)-K(5) /Al_2O_3	1%CO_2+3%O_2+ 2.5%H_2O/He	4%H_2/He	0.38	350	[3]
Ru(0.95)-Ca(5.1) /Al_2O_3	1%CO_2+3%O_2 +2.5%H_2O/He	4%H_2/He	0.48	350	[3]
Ru(0.84)-Ba(16) /Al_2O_3	1%CO_2+3%O_2 +2.5%H_2O/He	4%H_2/He	2.22	350	[3]
Ni(10)-Ca(30)/Al_2O_3	1%CO_2+10%O_2/N_2	100%H_2	0.15	450	[4]
Ni(10)/Al_2O_3	1%CO_2+10%O_2/N_2	100%H_2	0.002	450	[4]
Ni(10)-Ca(6)/Al_2O_3	1%CO_2+10%O_2/N_2	100%H_2	0.08	450	[4]
Ni(10)-Ca(20)/Al_2O_3	1%CO_2+10%O_2/N_2	100%H_2	0.09	450	[4]
Ni(10)-Ca(40)/Al_2O_3	1%CO_2+10%O_2/N_2	100%H_2	0.15	450	[4]
Ni(5)-Ca(30)/Al_2O_3	1%CO_2+10%O_2/N_2	100%H_2	0.13	450	[4]
Ni(20)-Ca(30)/Al_2O_3	1%CO_2+10%O_2/N_2	100%H_2	0.14	450	[4]
Ca(30)-Ni(10)/Al_2O_3	1%CO_2+10%O_2/N_2	100%H_2	0.064	450	[4]
Ni(10)/Al_2O_3	2.5%CO_2+10%O_2/N_2	100%H_2	0.43	500	[5]
Ni(10)/CaO	2.5%CO_2+10%O_2/N_2	100%H_2	20.4	500	[5]
Ni(10)-Ca(28)/Al_2O_3	2.5%CO_2+10%O_2/N_2	100%H_2	29.9	500	[5]
Ni(10)-Ca(8)/Al_2O_3	2.5%CO_2+10%O_2/N_2	100%H_2	8.66	500	[5]
Ni(10)-Ca(14)/Al_2O_3	2.5%CO_2+10%O_2/N_2	100%H_2	15.54	500	[5]
Ni(10)-Ca(32)/Al_2O_3	2.5%CO_2+10%O_2/N_2	100%H_2	24.1	500	[5]
Ni(30)-Ca(28)/Al_2O_3	2.5%CO_2+10%O_2/N_2	100%H_2	20.7	500	[5]
Ni(50)-Ca(28)/Al_2O_3	2.5%CO_2+10%O_2/N_2	100%H_2	22.63	500	[5]
Ni(10)-Ca(28)/Al_2O_3	2.5%CO_2+10%O_2/N_2	100%H_2	15.1	400	[5]
Ni(10)-Ca(28)/Al_2O_3	2.5%CO_2/10%O_2/N_2	100%H_2	5.91	300	[5]
Ni(10)-Ca(6)/Al_2O_3	0.25%CO_2+10%O_2/N_2	100%H_2	14.0	350	[6]
Ni_2Ca_2-Mg_2Al_2 /LDH	10%CO_2+5%O_2/He	20%H_2/He	15.68	320	[7]
Ni_2Ca_4-Al_2/LDH	10%CO_2+5%O_2/He	20%H_2/He	12.88	320	[7]

Ni_2Mg_2-Al_2-/LDH	10%CO_2+5%O_2/He	20%H_2/He	6.72	320	[7]
Ni(30)/CaO(15)-MgO(15)-Al_2O_3	10%CO_2+5%O_2/He	20%H_2/He	6.16	320	[7]
Ru(0.84)-Ba(16)/Al_2O_3	1%CO_2+3%O_2+2.5%H_2O/He	4%H_2/He	1.12	350	[8]
Ru(1)/Al_2O_3 + Ba(16)/Al_2O_3	1%CO_2+3%O_2+2.5%H_2O/He	4%H_2/He	0.63	350	[8]
Na-Ni/Al_2O_3	5%CO_2+4.5%O_2+11%H_2O/Ar	5%H_2/Ar	0.47	350	[9]
K-Ni/Al_2O_3	5%CO_2+11%H_2O+4.5%O_2/Ar	5%H_2/Ar	2.333	350	[9]
Ba-Ni/Al_2O_3	5%CO_2+11%H_2O+4.5%O_2/Ar	5%H_2/Ar	0.093	350	[9]
Ru(0.5)-Na_2O(6.1) /Al_2O_3	7.5%CO_2+4.5%O_2 +15%H_2O/N_2	15%H_2/N_2	13.44	320	[10]
Ru(1)-Na_2O(6.1) /Al_2O_3	7.5%CO_2+4.5%O_2 +15%H_2O/N_2	15%H_2/N_2	14.93	320	[10]
Ru(1)-Na/Al_2O_3	10%CO_2+10%O_2 +10%H_2O/He	10%H_2/Ar	2.6	300	[11]
Ru(1)-Na/Al_2O_3	10%CO_2+10%O_2/He	10%H_2/Ar	15.4	300	[11]
Ru(1)-Na/Al_2O_3	10%CO_2+10%O_2/He	10%H_2/Ar	24.3	300	[11]
HT-23NiR	7.5%CO_2+4.5%O_2/He	100%H_2	0.020	250	[12]
HT-23NiR	7.5%CO_2+4.5%O_2/He	100%H_2	0.028	300	[12]
HT-23NiR	7.5%CO_2+4.5%O_2/He	100%H_2	0.022	320	[12]
HT-46NiR	7.5%CO_2+4.5%O_2/He	100%H_2	0.032	250	[12]
HT-46NiR	7.5%CO_2+4.5%O_2/He	100%H_2	0.038	300	[12]
HT-46NiR	7.5%CO_2+4.5%O_2/He	100%H_2	0.032	320	[12]
Ni-Pr/CeO_2	10%CO_2+10%O_2/Ar	10%H_2/Ar	3.11	300	[13]
RuNi-Pr/CeO_2	10%CO_2+10%O_2/Ar	10%H_2/Ar	3.70	300	[13]

*This study

Supplementary Table 2. Summary of the reported CO_2 capture and methanation.

DFMs or catalyst	CO_2 capture gas	Hydrogenation gas	CH_4 yield [%]	*T* [°C]	ref
Ru(5)-Na_2CO_3(10)/Al_2O_3	5%CO_2/N_2	5%H_2/N_2	5.23	320	[14]
Ru(5)-K_2CO_3(10)/Al_2O_3	5%CO_2/N_2	5%H_2/N_2	4.53	320	[14]
Ni(1)/$CeCaCO_3$	15%CO_2/N_2	100%H_2	8.96	550	[15]
Ni(10)/CaO	15%CO_2/N_2	100%H_2	3.73	550	[15]
Ni(1)/CeO_2-CaOphy	15%CO_2/N_2	100%H_2	11.9	550	[15]
Ni(10)/g-Al_2O_3	5%CO_2/N_2	100%H_2	0.19	450	[16]
Ni(10)-Na(15)/g-Al_2O_3	5%CO_2/N_2	100%H_2	3.33	450	[16]
Ni(10)-K(15)/g-Al_2O_3	5%CO_2/N_2	100%H_2	2.51	450	[16]
Ni(10)-Ca(15)/g-Al_2O_3	5%CO_2/N_2	100%H_2	1.08	450	[16]
Ni(10)-Na(15)/g-Al_2O_3	5%CO_2/N_2	100%H_2	4.77	450	[16]
Ni(10)-Na(15)/g-Al_2O_3	0.04%CO_2/N_2	100%H_2	17.8	450	[16]
Ni(10)-Na(15)/g-Al_2O_3	0.01%CO_2/N_2	100%H_2	49.7	450	[16]
Ni(10)-Na(15)/g-Al_2O_3	2%CO_2/N_2	100%H_2	99	400	[17]
Ru(10)/CaO	1.4%CO_2/Ar	10%H_2/Ar	31.1	370	[18]
Ru(10)/Na_2CO_3	1.4%CO_2/Ar	10%H_2/Ar	48.9	370	[18]
Ru(5)/CaO	11%CO_2/Ar	10%H_2/Ar	2.04	280	[18]
Ru(5)/CaO	11%CO_2/Ar	10%H_2/Ar	1.95	310	[18]
Ru(5)/CaO	11%CO_2/Ar	10%H_2/Ar	1.87	340	[18]
Ru(5)/CaO	11%CO_2/Ar	10%H_2/Ar	1.70	370	[18]
Ru(5)/CaO	11%CO_2/Ar	10%H_2/Ar	1.53	400	[18]
Ru(10)/CaO	11%CO_2/Ar	10%H_2/Ar	3.39	280	[18]
Ru(10)/CaO	11%CO_2/Ar	10%H_2/Ar	3.56	310	[18]
Ru(10)/CaO	11%CO_2/Ar	10%H_2/Ar	3.73	340	[18]
Ru(10)/CaO	11%CO_2/Ar	10%H_2/Ar	3.90	370	[18]
Ru(10)/CaO	11%CO_2/Ar	10%H_2/Ar	4.07	400	[18]
Ru(15)/CaO	11%CO_2/Ar	10%H_2/Ar	3.05	280	[18]
Ru(15)/CaO	11%CO_2/Ar	10%H_2/Ar	4.50	310	[18]
Ru(15)/CaO	11%CO_2/Ar	10%H_2/Ar	5.43	340	[18]
Ru(15)/CaO	11%CO_2/Ar	10%H_2/Ar	6.11	370	[18]
Ru(15)/CaO	11%CO_2/Ar	10%H_2/Ar	6.45	400	[18]
Ru(5)/Na_2CO_3	11%CO_2/Ar	10%H_2/Ar	2.55	280	[18]
Ru(5)/Na_2CO_3	11%CO_2/Ar	10%H_2/Ar	2.21	310	[18]
Ru(5)/Na_2CO_3	11%CO_2/Ar	10%H_2/Ar	1.87	340	[18]
Ru(5)/Na_2CO_3	11%CO_2/Ar	10%H_2/Ar	1.70	370	[18]
Ru(5)/Na_2CO_3	11%CO_2/Ar	10%H_2/Ar	1.53	400	[18]

Ru(10)/Na_2CO_3	11%CO_2/Ar	10%H_2/Ar	6.11	280	[18]
Ru(10)/Na_2CO_3	11%CO_2/Ar	10%H_2/Ar	6.19	310	[18]
Ru(10)/Na_2CO_3	11%CO_2/Ar	10%H_2/Ar	6.11	340	[18]
Ru(10)/Na_2CO_3	11%CO_2/Ar	10%H_2/Ar	5.85	370	[18]
Ru(10)/Na_2CO_3	11%CO_2/Ar	10%H_2/Ar	5.18	400	[18]
Ru(15)/Na_2CO_3	11%CO_2/Ar	10%H_2/Ar	5.77	280	[18]
Ru(15)/Na_2CO_3	11%CO_2/Ar	10%H_2/Ar	6.11	310	[18]
Ru(15)/Na_2CO_3	11%CO_2/Ar	10%H_2/Ar	6.11	340	[18]
Ru(15)/Na_2CO_3	11%CO_2/Ar	10%H_2/Ar	6.02	370	[18]
Ru(15)/Na_2CO_3	11%CO_2/Ar	10%H_2/Ar	5.85	400	[18]
Ni(5)-CaO(15)/Al_2O_3	10%CO_2/Ar	10%H_2/Ar	1.70	520	[19]
Ni(10)-CaO(15)/Al_2O_3	10%CO_2/Ar	10%H_2/Ar	1.96	520	[19]
Ni(10)-CaO(15)/Al_2O_3 coimp	10%CO_2/Ar	10%H_2/Ar	2.05	520	[19]
Ni(15)-CaO(15)/Al_2O_3	10%CO_2/Ar	10%H_2/Ar	2.65	520	[19]
Ni(5)-CaO(15)/Al_2O_3	10%CO_2/Ar	10%H_2/Ar	1.31	480	[19]
Ni(10)-CaO(15)/Al_2O_3	10%CO_2/Ar	10%H_2/Ar	1.90	480	[19]
Ni(10)-CaO(15)/Al_2O_3 coimp	10%CO_2/Ar	10%H_2/Ar	1.87	480	[19]
Ni(15)-CaO(15)/Al_2O_3	10%CO_2/Ar	10%H_2/Ar	2.43	480	[19]
Ni(5)-CaO(15)/Al_2O_3	10%CO_2/Ar	10%H_2/Ar	1.4	440	[19]
Ni(10)-CaO(15)/Al_2O_3	10%CO_2/Ar	10%H_2/Ar	1.50	440	[19]
Ni(10)-CaO(15)/Al_2O_3 coimp	10%CO_2/Ar	10%H_2/Ar	1.50	440	[19]
Ni(15)-CaO(15)/Al_2O_3	10%CO_2/Ar	10%H_2/Ar	2.33	440	[19]
Ni(5)-CaO(15)/Al_2O_3	10%CO_2/Ar	10%H_2/Ar	1.4	400	[19]
Ni(10)-CaO(15)/Al_2O_3	10%CO_2/Ar	10%H_2/Ar	1.49	400	[19]
Ni(10)-CaO(15)/Al_2O_3 coimp	10%CO_2/Ar	10%H_2/Ar	1.31	400	[19]
Ni(15)-CaO(15)/Al_2O_3	10%CO_2/Ar	10%H_2/Ar	2.24	400	[19]
Ni(5)-CaO(15)/Al_2O_3	10%CO_2/Ar	10%H_2/Ar	1.31	360	[19]
Ni(10)-CaO(15)/Al_2O_3	10%CO_2/Ar	10%H_2/Ar	1.4	360	[19]
Ni(10)-CaO(15)/Al_2O_3 coimp	10%CO_2/Ar	10%H_2/Ar	0.93	360	[19]
Ni(15)-CaO(15)/Al_2O_3	10%CO_2/Ar	10%H_2/Ar	2.05	360	[19]
Ni(5)-CaO(15)/Al_2O_3	10%CO_2/Ar	10%H_2/Ar	0.93	320	[19]
Ni(10)-CaO(15)/Al_2O_3	10%CO_2/Ar	10%H_2/Ar	1.12	320	[19]
Ni(10)-CaO(15)/Al_2O_3 coimp	10%CO_2/Ar	10%H_2/Ar	0.47	320	[19]
Ni(15)-CaO(15)/Al_2O_3	10%CO_2/Ar	10%H_2/Ar	1.49	320	[19]
Ni(5)-CaO(15)/Al_2O_3	10%CO_2/Ar	10%H_2/Ar	0.19	280	[19]
Ni(10)-CaO(15)/Al_2O_3	10%CO_2/Ar	10%H_2/Ar	0.56	280	[19]
Ni(10)-CaO(15)/Al_2O_3 coimp	10%CO_2/Ar	10%H_2/Ar	0.19	280	[19]
Ni(15)-CaO(15)/Al_2O_3	10%CO_2/Ar	10%H_2/Ar	0.93	280	[19]

Ni(5)-Na_2CO_3(10)/Al_2O_3	10%CO_2/Ar	10%H_2/Ar	1.87	520	[19]
Ni(10)-Na_2CO_3(10)/Al_2O_3	10%CO_2/Ar	10%H_2/Ar	1.96	520	[19]
Ni(10)-Na_2CO_3(10)/Al_2O_3 coimp	10%CO_2/Ar	10%H_2/Ar	1.96	520	[19]
Ni(15)-Na_2CO_3(10)/Al_2O_3	10%CO_2/Ar	10%H_2/Ar	2.05	520	[19]
Ni(5)-Na_2CO_3(10)/Al_2O_3	10%CO_2/Ar	10%H_2/Ar	2.24	480	[19]
Ni(10)-Na_2CO_3(10)/Al_2O_3	10%CO_2/Ar	10%H_2/Ar	2.61	480	[19]
Ni(10)-Na_2CO_3(10)/Al_2O_3 coimp	10%CO_2/Ar	10%H_2/Ar	2.52	480	[19]
Ni(15)-Na_2CO_3(10)/Al_2O_3	10%CO_2/Ar	10%H_2/Ar	2.52	480	[19]
Ni(5)-Na_2CO_3(10)/Al_2O_3	10%CO_2/Ar	10%H_2/Ar	2.33	440	[19]
Ni(10)-Na_2CO_3(10)/Al_2O_3	10%CO_2/Ar	10%H_2/Ar	2.8	440	[19]
Ni(10)-Na_2CO_3(10)/Al_2O_3 coimp	10%CO_2/Ar	10%H_2/Ar	2.8	440	[19]
Ni(15)-Na_2CO_3(10)/Al_2O_3	10%CO_2/Ar	10%H_2/Ar	2.8	440	[19]
Ni(5)-Na_2CO_3(10)/Al_2O_3	10%CO_2/Ar	10%H_2/Ar	2.8	400	[19]
Ni(10)-Na_2CO_3(10)/Al_2O_3	10%CO_2/Ar	10%H_2/Ar	3.45	400	[19]
Ni(10)-Na_2CO_3(10)/Al_2O_3 coimp	10%CO_2/Ar	10%H_2/Ar	3.43	400	[19]
Ni(15)-Na_2CO_3(10)/Al_2O_3	10%CO_2/Ar	10%H_2/Ar	3.47	400	[19]
Ni(5)-Na_2CO_3(10)/Al_2O_3	10%CO_2/Ar	10%H_2/Ar	3.36	360	[19]
Ni(10)-Na_2CO_3(10)/Al_2O_3	10%CO_2/Ar	10%H_2/Ar	3.17	360	[19]
Ni(10)-Na_2CO_3(10)/Al_2O_3 coimp	10%CO_2/Ar	10%H_2/Ar	2.8	360	[19]
Ni(15)-Na_2CO_3(10)/Al_2O_3	10%CO_2/Ar	10%H_2/Ar	3.27	360	[19]
Ni(5)-Na_2CO_3(10)/Al_2O_3	10%CO_2/Ar	10%H_2/Ar	1.4	320	[19]
Ni(10)-Na_2CO_3(10)/Al_2O_3	10%CO_2/Ar	10%H_2/Ar	2.05	320	[19]
Ni(10)-Na_2CO_3(10)/Al_2O_3 coimp	10%CO_2/Ar	10%H_2/Ar	1.49	320	[19]
Ni(15)-Na_2CO_3(10)/Al_2O_3	10%CO_2/Ar	10%H_2/Ar	2.33	320	[19]
Ni(5)-Na_2CO_3(10)/Al_2O_3	10%CO_2/Ar	10%H_2/Ar	0.093	280	[19]
Ni(10)-Na_2CO_3(10)/Al_2O_3	10%CO_2/Ar	10%H_2/Ar	0.56	280	[19]
Ni(10)-Na_2CO_3(10)/Al_2O_3 coimp	10%CO_2/Ar	10%H_2/Ar	0.37	280	[19]
Ni(15)-Na_2CO_3(10)/Al_2O_3	10%CO_2/Ar	10%H_2/Ar	0.65	280	[19]
Ru(2.5)/CeO_2	65%CO_2/N_2	5%H_2/N_2	2.96	300	[20]
Ru(5)/CeO_2	65%CO_2/N_2	5%H_2/N_2	3.41	300	[20]
Ru(10)/CeO_2	65%CO_2/N_2	5%H_2/N_2	3.65	300	[20]
Ni(20)/MgO	10%CO_2/Ar	5%H_2/Ar	0.17	250	[21]
Ni(20)/MgO	10%CO_2/Ar	5%H_2/Ar	0.50	300	[21]
Ni(20)/MgO	10%CO_2/Ar	5%H_2/Ar	0.45	350	[21]
Ni(50)/MgO	10%CO_2/Ar	5%H_2/Ar	0.34	250	[21]
Ni(50)/MgO	10%CO_2/Ar	5%H_2/Ar	1.23	300	[21]
Ni(50)/MgO	10%CO_2/Ar	5%H_2/Ar	1.06	350	[21]
Ni(80)/MgO	10%CO_2/Ar	5%H_2/Ar	0.45	250	[21]

Ni(80)/MgO	10%CO_2/Ar	5%H_2/Ar	1.51	300	[21]
Ni(80)/MgO	10%CO_2/Ar	5%H_2/Ar	1.29	350	[21]
Com-Ni(50)/MgO	10%CO_2/Ar	5%H_2/Ar	0.017	250	[21]
Com-Ni(50)/MgO	10%CO_2/Ar	5%H_2/Ar	0.45	300	[21]
Com-Ni(50)/MgO	10%CO_2/Ar	5%H_2/Ar	0.039	350	[21]
Ni/CaO	10%CO_2/N_2	10%H_2/N_2	0.67	400	[22]
Ni/CaO-MgO	10%CO_2/N_2	10%H_2/N_2	0.69	400	[22]
Ni/CaO-MgO	10%CO_2/N_2	10%H_2/N_2	0.24	400	[22]
Ni/MgO	10%CO_2/N_2	10%H_2/N_2	0.15	400	[22]
AMS-Ni/MgO	65%CO_2/N_2	20%H_2/N_2	0.040	450	[23]
AMS-Ni/MgO	65%CO_2/N_2	60%H_2/N_2	0.052	450	[23]
AMS-Ni/MgO	65%CO_2/N_2	100%H_2	0.046	450	[23]
AMS-Ni/MgO	65%CO_2/N_2	100%H_2	0.034	400	[23]
AMS-Ni/MgO	65%CO_2/N_2	100%H_2	0.044	500	[23]
Ru(0.84)-Ba(16)/Al_2O_3	1%CO_2/He	4%H_2/He	2.06	350	[24]
Ru(1)/Al_2O_3 + Ba(16)/Al_2O_3	1%CO_2/He	4%H_2/He	1.32	350	[24]
Ru(1)/Al_2O_3	1%CO_2/He	4%H_2/He	0.027	350	[3]
Ru(0.99)-Li(1)/Al_2O_3	1%CO_2/He	4%H_2/He	0.027	350	[3]
Ru(0.97)-Na(3)/Al_2O_3	1%CO_2/He	4%H_2/He	0.63	350	[3]
Ru(0.95)-K(5)/Al_2O_3	1%CO_2/He	4%H_2/He	2.53	350	[3]
Ru(0.97)-Mg(3.2)/Al_2O_3	1%CO_2/He	4%H_2/He	0.054	350	[3]
Ru(0.95)-Ca(5.1)/Al_2O_3	1%CO_2/He	4%H_2/He	1.85	350	[3]
Ru(0.84)-Ba(16)/Al_2O_3	1%CO_2/He	4%H_2/He	3.02	350	[3]
Ru/rod-CeO_2-MgO	35%CO_2/N_2	5%H_2/N_2	0.22	300	[25]
Ru/particle-CeO_2-MgO	35%CO_2/N_2	5%H_2/N_2	0.24	300	[25]
Ru/cube-CeO_2-MgO	35%CO_2/N_2	5%H_2/N_2	0.032	300	[25]
Ni-Na_2CO_3/Al_2O_3	9.5%CO_2/N_2	10%H_2/N_2	1.12	320	[26]
Ni-CaO/Al_2O_3	9.5%CO_2/N_2	10%H_2/N_2	0.88	320	[26]
Li_4SiO_4@Ni(2.5)/CeO_2	15%CO_2/N_2	100%H_2	9.16	560	[27]
Li_4SiO_4@Ni(5)/CeO_2	15%CO_2/N_2	100%H_2	9.96	560	[27]
Li_4SiO_4@Ni(7.5)/CeO_2	15%CO_2/N_2	100%H_2	9.56	560	[27]
Na-Ni/Al_2O_3	5%CO_2/Ar	5%H_2/Ar	0.16	250	[28]
K-Ni/Al_2O_3	5%CO_2/Ar	5%H_2/Ar	0.17	250	[28]
Ba-Ni/Al_2O_3	5%CO_2/Ar	5%H_2/Ar	0.084	250	[28]
Na-Ni/Al_2O_3	5%CO_2/Ar	5%H_2/Ar	1.87	300	[28]
K-Ni/Al_2O_3	5%CO_2/Ar	5%H_2/Ar	2.43	300	[28]
Ba-Ni/Al_2O_3	5%CO_2/Ar	5%H_2/Ar	0.47	300	[28]

Ni/Al_2O_3	$5\%CO_2/Ar$	$5\%H_2/Ar$	0.47	300	[28]
$Na\text{-}Ni/Al_2O_3$	$5\%CO_2/Ar$	$5\%H_2/Ar$	3.17	350	[28]
$K\text{-}Ni/Al_2O_3$	$5\%CO_2/Ar$	$5\%H_2/Ar$	1.49	350	[28]
$Ba\text{-}Ni/Al_2O_3$	$5\%CO_2/Ar$	$5\%H_2/Ar$	0.93	350	[28]
$Na\text{-}Ni/Al_2O_3$	$5\%CO_2/Ar$	$5\%H_2/Ar$	2.61	400	[28]
$K\text{-}Ni/Al_2O_3$	$5\%CO_2/Ar$	$5\%H_2/Ar$	1.59	400	[28]
$Ba\text{-}Ni/Al_2O_3$	$5\%CO_2/Ar$	$5\%H_2/Ar$	0.75	400	[28]
$Na\text{-}Ni/Al_2O_3$	$5\%CO_2/Ar$	$5\%H_2/Ar$	2.89	450	[28]
$K\text{-}Ni/Al_2O_3$	$5\%CO_2/Ar$	$5\%H_2/Ar$	2.29	450	[28]
$Ba\text{-}Ni/Al_2O_3$	$5\%CO_2/Ar$	$5\%H_2/Ar$	0.65	450	[28]
$Ru(0.89)\text{-}Li(5)/Al_2O_3$	$10\%CO_2/N_2$	$10\%H_2/N_2$	2.02	280	[29]
$Ru(3)\text{-}K(10)/Al_2O_3$	$5\%CO_2/Ar$	$5\%H_2/Ar$	4.85	300	[29]
$Ru(3)\text{-}K(10)/Al_2O_3$	$5\%CO_2/Ar$	$5\%H_2/Ar$	0.93	350	[29]
$Ru(3)\text{-}K(10)/Al_2O_3$	$5\%CO_2/Ar$	$5\%H_2/Ar$	7.09	400	[29]
$Ru(3)\text{-}K(10)/Al_2O_3$	$5\%CO_2/Ar$	$5\%H_2/Ar$	4.57	450	[29]
$Ru(3)\text{-}Na(10)/Al_2O_3$	$5\%CO_2/Ar$	$5\%H_2/Ar$	10.4	300	[29]
$Ru(3)\text{-}Na(10)/Al_2O_3$	$5\%CO_2/Ar$	$5\%H_2/Ar$	9.15	350	[29]
$Ru(3)\text{-}Na(10)/Al_2O_3$	$5\%CO_2/Ar$	$5\%H_2/Ar$	7.65	400	[29]
$Ru(3)\text{-}Na(10)/Al_2O_3$	$5\%CO_2/Ar$	$5\%H_2/Ar$	3.45	450	[29]
$Ru(3)\text{-}Ba(10)/Al_2O_3$	$5\%CO_2/Ar$	$5\%H_2/Ar$	1.49	250	[29]
$Ru(3)\text{-}Ba(10)/Al_2O_3$	$5\%CO_2/Ar$	$5\%H_2/Ar$	6.35	300	[29]
$Ru(3)\text{-}Ba(10)/Al_2O_3$	$5\%CO_2/Ar$	$5\%H_2/Ar$	4.85	350	[29]
$Ru(3)\text{-}Ba(10)/Al_2O_3$	$5\%CO_2/Ar$	$5\%H_2/Ar$	2.05	400	[29]
$Ru(3)\text{-}Ba(10)/Al_2O_3$	$5\%CO_2/Ar$	$5\%H_2/Ar$	2.61	450	[29]
$Ru(1)\text{-}Na(20)/Al_2O_3$	$10\%CO_2/N_2$	$5\%H_2/N_2$	1.53	340	[30]
$Ru(0.5)\text{-}Na_2O(6.1)$ $/Al_2O_3$	$7.5\%CO_2/N_2$	$15\%H_2/N_2$	9.71	320	[31]
$Ru(0.5)\text{-}Na_2O(6.1)/Al_2O_3$	$7.5\%CO_2+$ $15\%H_2O/N_2$	$15\%H_2/N_2$	7.47	320	[31]
Ni/Hydrotalcite	$15\%CO_2/N_2$	$100\%H_2$	3.88	400	[32]
Ni/Hydrotalcite	$15\%CO_2/N_2$	$100\%H_2$	4.85	450	[32]
Ni/Hydrotalcite	$15\%CO_2/N_2$	$100\%H_2$	4.78	500	[32]
Ni/Hydrotalcite	$15\%CO_2/N_2$	$100\%H_2$	3.96	550	[32]
Ni/Hydrotalcite	$15\%CO_2/N_2$	$100\%H_2$	3.58	600	[32]
Ni-Cs(10)/Hydrotalcite	$15\%CO_2/N_2$	$100\%H_2$	4.93	350	[32]
Ni(1)/CaO	$15\%CO_2/N_2$	$100\%H_2$	2.99	550	[33]
Ni(10)/CaO	$15\%CO_2/N_2$	$100\%H_2$	3.73	550	[33]
Ni(1)/CeCaO	$15\%CO_2/N_2$	$100\%H_2$	4.93	550	[33]
Ni(1)/CeCaCO3	$15\%CO_2/N_2$	$100\%H_2$	8.96	550	[33]

Ni(1)/CeO_2 + CaO	15%CO_2/N_2	100%H_2	11.95	550	[33]
$LaNiO_3$(20)/CeO_2	10%CO_2/Ar	5%H_2/Ar	1.16	280	[34]
$LaNiO_3$(20)/CeO_2	10%CO_2/Ar	5%H_2/Ar	1.77	320	[34]
$LaNiO_3$(20)/CeO_2	10%CO_2/Ar	5%H_2/Ar	1.87	360	[34]
$LaNiO_3$(20)/CeO_2	10%CO_2/Ar	5%H_2/Ar	2.02	400	[34]
$LaNiO_3$(20)/CeO_2	10%CO_2/Ar	5%H_2/Ar	2.05	440	[34]
$LaNiO_3$(20)/CeO_2	10%CO_2/Ar	5%H_2/Ar	2.00	480	[34]
$LaNiO_3$(20)/CeO_2	10%CO_2/Ar	5%H_2/Ar	1.92	520	[34]
$La_{0.7}Ca_{0.3}NiO_3$(20)/CeO_2	10%CO_2/Ar	5%H_2/Ar	1.4	280	[34]
$La_{0.7}Ca_{0.3}NiO_3$(20)/CeO_2	10%CO_2/Ar	5%H_2/Ar	1.87	320	[34]
$La_{0.7}Ca_{0.3}NiO_3$(20)/CeO_2	10%CO_2/Ar	5%H_2/Ar	2.24	360	[34]
$La_{0.7}Ca_{0.3}NiO_3$(20)/CeO_2	10%CO_2/Ar	5%H_2/Ar	2.39	400	[34]
$La_{0.7}Ca_{0.3}NiO_3$(20)/CeO_2	10%CO_2/Ar	5%H_2/Ar	2.61	440	[34]
$La_{0.7}Ca_{0.3}NiO_3$(20)/CeO_2	10%CO_2/Ar	5%H_2/Ar	2.8	480	[34]
$La_{0.7}Ca_{0.3}NiO_3$(20)/CeO_2	10%CO_2/Ar	5%H_2/Ar	2.37	520	[34]
$La_{0.7}Ba_{0.3}NiO_3$(20)/CeO_2	10%CO_2/Ar	5%H_2/Ar	1.16	280	[34]
$La_{0.7}Ba_{0.3}NiO_3$(20)/CeO_2	10%CO_2/Ar	5%H_2/Ar	1.77	320	[34]
$La_{0.7}Ba_{0.3}NiO_3$(20)/CeO_2	10%CO_2/Ar	5%H_2/Ar	2.02	360	[34]
$La_{0.7}Ba_{0.3}NiO_3$(20)/CeO_2	10%CO_2/Ar	5%H_2/Ar	2.05	400	[34]
$La_{0.7}Ba_{0.3}NiO_3$(20)/CeO_2	10%CO_2/Ar	5%H_2/Ar	1.98	440	[34]
$La_{0.7}Ba_{0.3}NiO_3$(20)/CeO_2	10%CO_2/Ar	5%H_2/Ar	1.59	480	[34]
$La_{0.7}Ba_{0.3}NiO_3$(20)/CeO_2	10%CO_2/Ar	5%H_2/Ar	1.4	520	[34]
$La_{0.7}Na_{0.3}NiO_3$(20)/CeO_2	10%CO_2/Ar	5%H_2/Ar	1.08	280	[34]
$La_{0.7}Na_{0.3}NiO_3$(20)/CeO_2	10%CO_2/Ar	5%H_2/Ar	1.21	320	[34]
$La_{0.7}Na_{0.3}NiO_3$(20)/CeO_2	10%CO_2/Ar	5%H_2/Ar	1.30	360	[34]
$La_{0.7}Na_{0.3}NiO_3$(20)/CeO_2	10%CO_2/Ar	5%H_2/Ar	1.16	400	[34]
$La_{0.7}Na_{0.3}NiO_3$(20)/CeO_2	10%CO_2/Ar	5%H_2/Ar	1.10	440	[34]
$La_{0.7}Na_{0.3}NiO_3$(20)/CeO_2	10%CO_2/Ar	5%H_2/Ar	1.03	480	[34]
$La_{0.7}Na_{0.3}NiO_3$(20)/CeO_2	10%CO_2/Ar	5%H_2/Ar	0.75	520	[34]
$La_{0.7}K_{0.3}NiO_3$(20)/CeO_2	10%CO_2/Ar	5%H_2/Ar	0.65	280	[34]
$La_{0.7}K_{0.3}NiO_3$(20)/CeO_2	10%CO_2/Ar	5%H_2/Ar	0.896	320	[34]
$La_{0.7}K_{0.3}NiO_3$(20)/CeO_2	10%CO_2/Ar	5%H_2/Ar	0.93	360	[34]
$La_{0.7}K_{0.3}NiO_3$(20)/CeO_2	10%CO_2/Ar	5%H_2/Ar	0.93	400	[34]
$La_{0.7}K_{0.3}NiO_3$(20)/CeO_2	10%CO_2/Ar	5%H_2/Ar	0.91	440	[34]
$La_{0.7}K_{0.3}NiO_3$(20)/CeO_2	10%CO_2/Ar	5%H_2/Ar	0.90	480	[34]
$La_{0.7}K_{0.3}NiO_3$(20)/CeO_2	10%CO_2/Ar	5%H_2/Ar	0.84	520	[34]
Ru/CeO_2-$CaCO_3$	20%CO_2/N_2	100%H_2	1.79	350	[35]

Ru/CeO_2-KNO_3 $CaCO_3$	20%CO_2/N_2	100%H_2	2.52	350	[35]
Ru/CeO_2-$LiNO_3$ $CaCO_3$	20%CO_2/N_2	100%H_2	1.456	350	[35]
Ru/CeO_2-(Li-K)NO_3 $CaCO_3$	20%CO_2/N_2	100%H_2	2.184	350	[35]
Ru/CeO_2-KNO_3 $CaCO_3$	20%CO_2/N_2	100%H_2	3.192	400	[35]
Ru/CeO_2-KNO_3 $CaCO_3$	20%CO_2/N_2	100%H_2	5.32	450	[35]
Ru/CeO_2-KNO_3 $CaCO_3$	20%CO_2/N_2	100%H_2	3.81	500	[35]
Ru(0.25)-Na/Al_2O_3	10%CO_2/Ar	10%H_2/Ar	0.72	300	[36]
Ru(0.5)-Na/Al_2O_3	10%CO_2/Ar	10%H_2/Ar	2.27	300	[36]
Ru(1)-Na/Al_2O_3	10%CO_2/Ar	10%H_2/Ar	2.688	300	[36]
Ru(2)-Na/Al_2O_3	10%CO_2/Ar	10%H_2/Ar	2.68	300	[36]
Ru(4)-Na/Al_2O_3	10%CO_2/Ar	10%H_2/Ar	2.66	300	[36]
Ni-Pr/CeO_2	10%CO_2/Ar	10%H_2/Ar	4.66	300	[13]
RuNi-Pr/CeO_2	10%CO_2/Ar	10%H_2/Ar	5.62	300	[13]
Ni/MgO	65%CO_2/N_2	50%H_2/N_2	0.046	500	[37]

Supplementary Table 3. Summary of the continuous CO_2 capture and RWGS reaction in this study and other reported CO_2 capture and RWGS reaction considering the effect of coexistent O_2.

DFMs or catalyst	CO_2 capture gas	Hydrogenation gas	CO yield [%]	*T* [°C]	ref
$Cu/ZnO/Al_2O_3$	$10\%CO_2+10\%O_2/He$	$100\%H_2$	85.1	650	*
$Pt(1)-Na(3)/Al_2O_3$	$1\%CO_2+10\%O_2/N_2$	$5\%H_2/N_2$	8.8	350	[38]
$Pt(1)-Na(3)/MgO$	$1\%CO_2+10\%O_2/N_2$	$5\%H_2/N_2$	3.4	350	[38]
$Pt(1)-Ca(6)/Al_2O_3$	$1\%CO_2+10\%O_2/N_2$	$5\%H_2/N_2$	2.3	350	[38]
$Pt(1)-Mg(3)/Al_2O_3$	$1\%CO_2/10\%O_2/N_2$	$5\%H_2/N_2$	0.56	450	[38]
$Pt(1)-K(6)/Al_2O_3$	$1\%CO_2+10\%O_2/N_2$	$5\%H_2/N_2$	0.39	450	[38]
$Ru(1)-Na(3)/Al_2O_3$	$1\%CO_2+10\%O_2/N_2$	$5\%H_2/N_2$	0.34	450	[38]
$Cu(1)-Na(3)/Al_2O_3$	$1\%CO_2+10\%O_2/N_2$	$5\%H_2/N_2$	0.17	450	[38]
$Pt(1)-Na(3)/SiO_2$	$1\%CO_2+10\%O_2/N_2$	$5\%H_2/N_2$	0.34	450	[38]
$Pt(1)-Na(3)/TiO_2$	$1\%CO_2+10\%O_2/N_2$	$5\%H_2/N_2$	1.68	450	[38]
$Rb-Ni/Al_2O_3$	$0.5\%CO_2+10\%O_2/N_2$	$20\%H_2/N_2$	47.8	450	[39]
$Pt-Na/Al_2O_3$	$0.5\%CO_2+10\%O_2/N_2$	$20\%H_2/N_2$	34.7	450	[39]
$Ni-Rb/Al_2O_3$	$0.5\%CO_2+10\%O_2/N_2$	$20\%H_2/N_2$	28.2	450	[39]
$Na-Ni/Al_2O_3$	$0.5\%CO_2+10\%O_2/N_2$	$20\%H_2/N_2$	12.9	450	[39]
$Mg-Ni/Al_2O_3$	$0.5\%CO_2+10\%O_2/N_2$	$20\%H_2/N_2$	0.54	450	[39]
Na/Al_2O_3	$0.5\%CO_2+10\%O_2/N_2$	$20\%H_2/N_2$	15.1	450	[39]
Rb/Al_2O_3	$0.5\%CO_2+10\%O_2/N_2$	$20\%H_2/N_2$	16.1	450	[39]
Fe(6.91)Cr(0.58)Cu(0.20)-K(9.98)/hydrotalcite	$5.8\%CO_2+5\%O_2+4\%H_2O/N_2$	$100\%H_2$	41.3	450	[40]
Fe(6.91)Cr(0.58)Cu(0.20)-K(9.98)/hydrotalcite	$5.8\%CO_2+5\%O_2+4\%H_2O/N_2$	$100\%H_2$	52.2	500	[40]
Fe(6.91)Cr(0.58)Cu(0.20)-K(9.98)/hydrotalcite	$5.8\%CO_2+5\%O_2+4\%H_2O/N_2$	$100\%H_2$	56.0	530	[40]

*This study

Supplementary Table 4. Summary of reported CO_2 capture and RWGS reaction.

DFMs or catalyst	CO_2 capture gas	Hydrogenation gas	CO yield. [%]	*T* [°C]	ref
$Ca_1Ni_{0.1}O$	15%CO_2/N_2	5%H_2/N_2	10.3	650	41
$Ca_1Ni_{0.1}Ce_{0.017}O$	15%CO_2/N_2	5%H_2/N_2	10.8	650	41
$Ca_1Ni_{0.1}Ce_{0.033}O$	15%CO_2/N_2	5%H_2/N_2	10.9	650	41
Fe(5)Co(5)Mg(10)/CaO	10%CO_2/He	100%H_2	30.9	650	42
CaO	10%CO_2/He	100%H_2	10.3	650	42
Fe(10)Mg(10)/CaO	10%CO_2/He	100%H_2	26.9	650	42
Fe(8)Co(2)Mg(10)CaO	10%CO_2/He	100%H_2	26.5	650	42
Fe(7.5)Co(2.5)Mg(10)CaO	10%CO_2/He	100%H_2	27.7	650	42
Fe(6.7)Co(3.3)Mg(10)CaO	10%CO_2/He	100%H_2	29.7	650	42
Fe(3.3)Co(6.7)Mg(10)CaO	10%CO_2/He	100%H_2	26.0	650	42
Co(10)Mg(10)CaO	10%CO_2/He	100%H_2	24.4	650	42
Ni(10)/CaO	10%CO_2/N_2	5%H_2/N_2	10.6	650	43
Ni(10)/Carbide slag(CS)	10%CO_2/N_2	5%H_2/N_2	10.6	650	43
Rb-Ni/Al_2O_3	0.5%CO_2/N_2	20%H_2/N_2	22.0	450	39
Ni(10)/CaZr(O)	15%CO_2/N_2	66.7%H_2/N_2	4.80	600	44
Ni(10)/CaAl(O)	15%CO_2/N_2	66.7%H_2/N_2	6.95	600	44
Ni(10)/CaO	15%CO_2/N_2	66.7%H_2/N_2	6.09	600	44
Ni(10)/CaMg(O)	15%CO_2/N_2	66.7%H_2/N_2	5.37	600	44
Cu(11)-K(10)/Al_2O_3	4.4%CO_2/He	100%H_2	27.6	450	45
Fe(6.91)Cr(0.58)Cu(0.20)-K(9.98)/hydrotalcite	5.8%CO_2/N_2	100%H_2	72.7	550	40
Fe(6.91)Cr(0.58)Cu(0.20)-K(9.98)/hydrotalcite	5.8%CO_2+4%H_2O/N_2	100%H_2	64.3	550	40
Fe(6.91)Cr(0.58)Cu(0.20)-K(9.98)/hydrotalcite	5.8%CO_2/4%O_2/N_2	100%H_2	50.8	550	40
Fe(6.91)Cr(0.58)Cu(0.20)-K(9.98)/hydrotalcite	7.6%CO_2/N_2	100%H_2	54.7	550	40
Fe(6.91)Cr(0.58)Cu(0.20)-K(9.98)/hydrotalcite	7.6%CO_2/4%H_2O/N_2	100%H_2	44.9	550	40
Fe(6.91)Cr(0.58)Cu(0.20)-K(9.98)/hydrotalcite	9.5%CO_2/N_2	100%H_2	38.7	550	40
Fe(6.91)Cr(0.58)Cu(0.20)-K(9.98)/hydrotalcite	9.5%CO_2/4%H_2O/N_2	100%H_2	32.4	550	40
Fe(6.91)Cr(0.58)Cu(0.20)-K(9.98)/hydrotalcite	5.8%CO_2/N_2	100%H_2	72.3	450	40
Fe(6.91)Cr(0.58)Cu(0.20)-K(9.98)/hydrotalcite	5.8%CO_2/N_2	100%H_2	72.7	470	40
Fe(6.91)Cr(0.58)Cu(0.20)-K(9.98)/hydrotalcite	5.8%CO_2/N_2	100%H_2	78.5	500	40
Fe(6.91)Cr(0.58)Cu(0.20)-K(9.98)/hydrotalcite	5.8%CO_2/N_2	100%H_2	83.1	530	40
Na(16)/Al_2O_3	5%CO_2/N_2	100%H_2	5.08	450	46
K(21)/Al_2O_3	5%CO_2/N_2	100%H_2	5.97	450	46

Ca(15)/Al_2O_3	5%CO_2/N_2	100%H_2	2.7	450	[46]
Al_2O_3	5%CO_2/N_2	100%H_2	0.30	450	[46]
Na(16)/Al_2O_3	5%CO_2/N_2	100%H_2	2.33	350	[46]
Na(16)/Al_2O_3	5%CO_2/N_2	100%H_2	4.928	400	[46]
Na(16)/Al_2O_3	5%CO_2/N_2	100%H_2	5.36	500	[46]
CaO	15%CO_2/N_2	15%H_2	1.58	600	[47]
CaO	15%CO_2/N_2	15%H_2	7.1	650	[47]
CaO	15%CO_2/N_2	15%H_2	19.3	700	[47]
CeO_2(33)/CaO	17%CO_2/N_2	5%H_2/N_2	2.16	650	[47]
CeO_2(33)/CaO	17%CO_2/N_2	5%H_2/N_2	0.98	600	[47]
CeO_2(33)/CaO	17%CO_2/N_2	5%H_2/N_2	3.63	700	[47]
CeO_2(33)/CaO	17%CO_2/N_2	5%H_2/N_2	1.81	750	[47]
CeO_2(10)/CaO	17%CO_2/N_2	5%H_2/N_2	0.84	600	[47]
CeO_2(10)/CaO	17%CO_2/N_2	5%H_2/N_2	3.56	650	[47]
CeO_2(10)/CaO	17%CO_2/N_2	5%H_2/N_2	4.88	700	[47]
CeO_2(10)/CaO	17%CO_2/N_2	5%H_2/N_2	2.23	750	[47]
CeO_2(16)/CaO	17%CO_2/N_2	5%H_2/N_2	0.70	600	[47]
CeO_2(16)/CaO	17%CO_2/N_2	5%H_2/N_2	2.51	650	[47]
CeO_2(16)/CaO	17%CO_2/N_2	5%H_2/N_2	4.74	700	[47]
CeO_2(16)/CaO	17%CO_2/N_2	5%H_2/N_2	2.65	750	[47]
CeO_2(50)/CaO	17%CO_2/N_2	5%H_2/N_2	0.56	600	[47]
CeO_2(50)/CaO	17%CO_2/N_2	5%H_2/N_2	2.23	650	[47]
CeO_2(50)/CaO	17%CO_2/N_2	5%H_2/N_2	2.93	700	[47]
CeO_2(50)/CaO	17%CO_2/N_2	5%H_2/N_2	0.84	750	[47]
CeO_2(67)/CaO	17%CO_2/N_2	5%H_2/N_2	0.35	600	[47]
CeO_2(67)/CaO	17%CO_2/N_2	5%H_2/N_2	1.39	650	[47]
CeO_2(67)/CaO	17%CO_2/N_2	5%H_2/N_2	1.39	700	[47]
CeO_2(67)/CaO	17%CO_2/N_2	5%H_2/N_2	0.56	750	[47]
Ni/CaO	10%CO_2/10%H_2O/N_2	10%H_2/N_2	21.5	700	[48]
La(15)-Ni(2.5)/CaO	10%CO_2/Ar	10%H_2/Ar	43.3	650	[49]
Mg(15)-Ni(2.5)/CaO	10%CO_2/Ar	10%H_2/Ar	38.8	650	[49]
Zr(15)-Ni(2.5)/CaO	10%CO_2/Ar	10%H_2/Ar	36.3	650	[49]
Ce(15)-Ni(2.5)/CaO	10%CO_2/Ar	10%H_2/Ar	41.3	650	[49]
Ni(2.5)/CaO	10%CO_2/Ar	10%H_2/Ar	31.36	650	[49]

References

1. Arellano-Treviño, M. A., Kanani, N., Jeong-Potter, C. W. & Farrauto, R. J. Bimetallic catalysts for CO_2 capture and hydrogenation at simulated flue gas conditions. *Chem. Eng. J.* **375**, (2019).
2. Arellano-Treviño, M. A., He, Z., Libby, M. C. & Farrauto, R. J. Catalysts and adsorbents for CO2 capture and conversion with dual function materials: Limitations of Ni-containing DFMs for flue gas applications. *J. CO2 Util.* **31**, 143–151 (2019).
3. Porta, A., Matarrese, R., Visconti, C. G., Castoldi, L. & Lietti, L. Storage Material Effects on the Performance of Ru-Based CO2Capture and Methanation Dual Functioning Materials. *Ind Eng Chem Res* **60**, 6706–6718 (2021).
4. Li, L. *et al.* Continuous CO2 capture and methanation over Ni-Ca/Al2O3 dual functional materials. *RSC Adv* **13**, 2213–2219 (2023).
5. Miyazaki, S. *et al.* In Situ Spectroscopic Study of CO2 Capture and Methanation over Ni−Ca Based Dual Functional Materials. *Chem Asian J* (2023) doi:10.1002/asia.202301003.
6. Li, L. *et al.* Continuous direct air capture and methanation using combined system of membrane-based CO2 capture and Ni-Ca based dual functional materials. *Appl Catal B* **339**, (2023).
7. Sakai, M., Imagawa, H. & Baba, N. Layered-double-hydroxide-based Ni catalyst for CO2 capture and methanation. *Appl Catal A Gen* **647**, (2022).
8. Porta, A. *et al.* Ru-Ba synergistic effect in dual functioning materials for cyclic CO2 capture and methanation. *Appl Catal B* **283**, (2021).
9. García-Bordejé, E., Belén Dongil, A., Conesa, J. M., Guerrero-Ruiz, A. & Rodríguez-Ramos, I. Dual functional materials based on Ni and different alkaline metals on alumina for the cyclic stepwise CO2 capture and methanation. *Chemical Engineering Journal* **472**, (2023).
10. Jeong-Potter, C. *et al.* Aging study of low Ru loading dual function materials (DFM) for combined power plant effluent CO2 capture and methanation. *Appl Catal B* **310**, (2022).
11. Tsiotsias, A. I. *et al.* CO2 capture and methanation using Ru/Na2O/Al2O3 dual-function materials: Effect of support synthesis method and Ru load. *J Environ Chem Eng* **12**, (2024).
12. Marin, J., Parra, P. & Rios, L. Improved Dual Function Materials for CO2 Capture and In Situ Methanation. *Energy Technology* **12**, (2024).
13. Tsiotsias, A. I. *et al.* Integrating capture and methanation of CO2 using physical mixtures of Na-Al2O3 and mono-/ bimetallic (Ru)Ni/Pr-CeO2. *Chemical Engineering Journal* **491**, (2024).
14. Duyar, M. S., Wang, S., Arellano-Treviño, M. A. & Farrauto, R. J. CO2 utilization with a novel dual function material (DFM) for capture and catalytic conversion to synthetic natural gas: An update. *Journal of CO2 Utilization* **15**, 65–71 (2016).
15. Sun, H. *et al.* Understanding the interaction between active sites and sorbents during the integrated carbon capture and utilization process. *Fuel* **286**, (2021).
16. Kosaka, F. *et al.* Enhanced Activity of Integrated CO2Capture and Reduction to CH4under Pressurized Conditions toward Atmospheric CO2Utilization. *ACS Sustain Chem Eng* **9**, 3452–3463 (2021).
17. Kosaka, F. *et al.* Direct and continuous conversion of flue gas CO2 into green fuels using dual function materials in a circulating fluidized bed system. *Chemical Engineering Journal* **450**, (2022).
18. Bermejo-López, A., Pereda-Ayo, B., González-Marcos, J. A. & González-Velasco, J. R. Mechanism of the CO2 storage and in situ hydrogenation to CH4. Temperature and adsorbent loading effects over Ru-CaO/Al2O3 and Ru-Na2CO3/Al2O3 catalysts. *Appl Catal B* **256**, (2019).
19. Bermejo-López, A., Pereda-Ayo, B., González-Marcos, J. A. & González-Velasco, J. R. Ni loading effects on dual function materials for capture and in-situ conversion of CO2 to CH4 using CaO or Na2CO3. *Journal of CO2 Utilization* **34**, 576–587 (2019).
20. Sun, H., Zhang, Y., Guan, S., Huang, J. & Wu, C. Direct and highly selective conversion of captured CO2into methane through integrated carbon capture and utilization over dual functional materials. *Journal of CO2*

Utilization **38**, 262–272 (2020).
21. Guo, Z. K. *et al.* Mechanochemical synthesis of Ni/MgO dual functional materials at room temperature for CO2 capture and methanation. *Chemical Engineering Journal* **481**, (2024).
22. Wu, X. *et al.* An investigation of the Ni/carbonate interfaces on dual function materials in integrated CO2 capture and utilisation cycles. *Appl Catal B* **338**, (2023).
23. Huang, P. *et al.* Influence of reduction conditions on the structure-activity relationships of NaNO3-promoted Ni/MgO dual function materials for integrated CO2 capture and methanation. *Chemical Engineering Journal* **467**, (2023).
24. Porta, A. *et al.* Ru-Ba synergistic effect in dual functioning materials for cyclic CO2 capture and methanation. *Appl Catal B* **283**, (2021).
25. Sun, S., Sun, H., Guan, S., Xu, S. & Wu, C. Integrated CO2 capture and methanation on Ru/CeO2-MgO combined materials: Morphology effect from CeO2 support. *Fuel* **317**, (2022).
26. Chai, K. H., Leong, L. K., Wong, D. S. H., Tsai, D. H. & Sethupathi, S. Effect of CO2 adsorbents on the Ni-based dual-function materials for CO2 capturing and in situ methanation. *Journal of the Chinese Chemical Society* **67**, 998–1008 (2020).
27. Lv, Z. *et al.* Integrated CO2 capture and In-Situ methanation by efficient dual functional Li4SiO4@Ni/CeO2. *Sep Purif Technol* **309**, (2023).
28. García-Bordejé, E., Belén Dongil, A., Conesa, J. M., Guerrero-Ruiz, A. & Rodríguez-Ramos, I. Dual functional materials based on Ni and different alkaline metals on alumina for the cyclic stepwise CO2 capture and methanation. *Chemical Engineering Journal* **472**, (2023).
29. García-Bordejé, E. *et al.* Cyclic performance in CO2capture-methanation of bifunctional Ru with different base metals: Effect of the reactivity of COx ad-species. *Journal of CO2 Utilization* **68**, (2023).
30. Chen, L., Liu, D. & Wei, G. Performance of Na-Ru/Al2O3 dual function material for integrated CO2 capture and methanation with the presence of coal ashes. *Energy Convers Manag* **299**, (2024).
31. Jeong-Potter, C. & Farrauto, R. Feasibility Study of Combining Direct Air Capture of CO2 and Methanation at Isothermal Conditions with Dual Function Materials. *Appl Catal B* **282**, (2021).
32. Faria, A. C. *et al.* Cyclic operation of CO2 capture and conversion into methane on Ni-hydrotalcite based dual function materials (DFMs). *Journal of CO2 Utilization* **72**, (2023).
33. Sun, H. *et al.* Understanding the interaction between active sites and sorbents during the integrated carbon capture and utilization process. *Fuel* **286**, (2021).
34. Onrubia-Calvo, J. A., Pereda-Ayo, B., González-Marcos, J. A. & González-Velasco, J. R. Lanthanum partial substitution by basic cations in LaNiO3/CeO2 precursors to raise DFM performance for integrated CO2 capture and methanation. *Journal of CO2 Utilization* **81**, (2024).
35. Wei, L. *et al.* Nitrate-promoted gas–solid reactions of H2 and CaCO3 for mid-temperature integrated CO2 capture and methanation. *Chemical Engineering Journal* **493**, (2024).
36. Tsiotsias, A. I. *et al.* CO2 capture and methanation using Ru/Na2O/Al2O3 dual-function materials: Effect of support synthesis method and Ru load. *J Environ Chem Eng* **12**, (2024).
37. Huang, P., Chu, J., Zhang, Z., Zhao, C. & Guo, Y. Optimizing alkali metal Salt-Induced structural assembly of Ni-MgO dual function materials for enhanced CO2 capture and methanation performance. *Chem Eng Sci* **294**, (2024).
38. Li, L. *et al.* Continuous CO 2 Capture and Selective Hydrogenation to CO over Na-Promoted Pt Nanoparticles on Al 2 O 3. *ACS Catal* **12**, 2639–2650 (2022).
39. Li, L. *et al.* Rb-Ni/Al2O3 as dual functional material for continuous CO2 capture and selective hydrogenation to CO. *Chemical Engineering Journal* **477**, (2023).
40. Bobadilla, L. F., Riesco-García, J. M., Penelás-Pérez, G. & Urakawa, A. Enabling continuous capture and catalytic conversion of flue gas CO2 to syngas in one process. *Journal of CO2 Utilization* **14**, 106–111 (2016).

41. Sun, H. *et al.* Dual functional catalytic materials of Ni over Ce-modified CaO sorbents for integrated CO2 capture and conversion. *Appl Catal B* **244**, 63–75 (2019).
42. Shao, B. *et al.* Heterojunction-redox catalysts of Fe: XCoyMg10CaO for high-temperature CO2capture and in situ conversion in the context of green manufacturing. *Energy Environ Sci* **14**, 2291–2301 (2021).
43. Wang, G. *et al.* Ni-CaO dual function materials prepared by different synthetic modes for integrated CO2 capture and conversion. *Chemical Engineering Journal* **428**, (2022).
44. Ma, X. *et al.* Metal oxide-doped Ni/CaO dual-function materials for integrated CO2 capture and conversion: Performance and mechanism. *AIChE Journal* **69**, (2023).
45. Hyakutake, T., Van Beek, W. & Urakawa, A. Unravelling the nature, evolution and spatial gradients of active species and active sites in the catalyst bed of unpromoted and K/Ba-promoted Cu/Al2O3 during CO2 capture-reduction. *J Mater Chem A Mater* **4**, 6878–6885 (2016).
46. Sasayama, T. *et al.* Integrated CO2capture and selective conversion to syngas using transition-metal-free Na/Al2O3dual-function material. *Journal of CO2 Utilization* **60**, (2022).
47. Sun, S. *et al.* Integrated CO2 capture and utilization with CaO-alone for high purity syngas production. *Carbon Capture Science and Technology* **1**, (2021).
48. Jo, S. Bin *et al.* CO2green technologies in CO2capture and direct utilization processes: methanation, reverse water-gas shift, and dry reforming of methane. *Sustain Energy Fuels* **4**, 5543–5549 (2020).
49. Hu, Y. *et al.* MxOy (M = Mg, Zr, La, Ce) modified Ni/CaO dual functional materials for combined CO2 capture and hydrogenation. *Int J Hydrogen Energy* **48**, 24871–24883 (2023).